2020

Comparisons of calretinin and parvalbumin neuronal distribution, density and inhibitory synapses in rhesus monkey prefrontal cortex and primary visual cortex and the analogous areas of mice

BOSTON UNIVERSITY

SCHOOL OF MEDICINE

Thesis

COMPARISONS OF CALRETININ AND PARVALBUMIN NEURONAL DISTRIBUTION, DENSITY AND INHIBITORY SYNAPSES IN RHESUS MONKEY PREFRONTAL CORTEX AND PRIMARY VISUAL CORTEX AND THE ANALOGOUS AREAS OF MICE

by

RAKIN TAMMAM NASAR

B.S., Wake Forest University, 2014

Submitted in partial fulfillment of the

requirements for the degree of

Master of Science

2020

Approved by

First Reader _____

Jennifer Luebke, Ph.D.
Professor of Anatomy & Neurobiology

Second Reader _____

Maria Medalla, Ph.D.
Assistant Professor of Anatomy & Neurobiology

ACKNOWLEDGMENTS

To my family for supporting me throughout my journey by making sure I stick to my priorities and that I have good intentions. You have supported me whenever I wanted to pursue something, whether that be a hobby or my career pursuits.

To my friends for giving me many smiles. In particular, my best friend Kevin and I talk every day; you keeps me motivated and gives me advice on all of my big decisions.

My Lab experience has been a complete delight thanks to all the people in the lab: Anna R, Joe, Alexa, Chelsea, Wayne, Emma, Diego, Sarah, Yuxin, Dhruba, Chrome, Dickson and Louis. You all make me look forward to coming into lab even when it is snowing or pouring rain. It has been amazing working with Louis, you are a diligent worker and your suggestions for food and entertainment have all been fantastic.

To Dr. Maria Medalla for being an incredibly thoughtful, passionate, and knowledgeable mentor. Your time and knowledge are one of the most sought after resources in the lab, and I am fortunate to have worked with you. I am especially grateful for one late Friday night in the lab when you bought us Tasty Burger, I didn't eat much that day and I didn't realize how hungry I was. You sincerely care about your students.

To Dr. Luebke for being a phenomenal mentor, teacher, and friend. Working with you has been one of the most formative and rewarding experiences of my life. You prioritized my personal, professional, and scientific growth. You pushed me to improve to levels that I didn't think were possible for me. On top of being a great scientist, your compassion and commitment to making the world a more just place is infectious. Working in your lab has been my favorite part of the program, thank you for that.

COMPARISONS OF CALRETININ AND PARVALBUMIN NEURONAL DISTRIBUTION, DENSITY AND INHIBITORY SYNAPSES IN RHESUS MONKEY PREFRONTAL CORTEX AND PRIMARY VISUAL CORTEX AND THE ANALOGOUS AREAS OF MICE

RAKIN TAMMAM NASAR

ABSTRACT

Calretinin (CR) and parvalbumin (PV) neurons are inhibitory interneurons (INs) that play important roles in the modulation of excitatory pyramidal neurons. They are found in many species are and throughout the neocortex. However, their characteristics vary between species and brain region. The aim of this study was to compare the density, distribution, and inhibitory signaling of CR and PV neurons in monkey primary visual cortex (V1), monkey lateral prefrontal cortex (LPFC), mouse V1 and mouse frontal cortex (FC). Coronal brain slices from each of the species and brain regions were stained using immunohistochemistry and then the slices were scanned using high-resolution confocal imaging. High resolution image stacks were used to count the somata of CR and PV. The vesicular gamma aminobutyric acid (GABA) transporter (VGAT), CR and PV particles were analyzed to quantify these inhibitory markers in monkey V1, LPFC, and mouse V1 and FC. There were significant differences in the laminar distribution of CR and PV neurons in that CR neurons were concentrated in L2/3 and PV neurons were concentrated in L2-5. In L2/3, Monkey V1 had more CR neurons than did monkey LPFC. Furthermore, there were a greater number of PV neurons in monkey and mouse V1 compared to monkey LPFC and mouse FC. In L2/3, monkey V1 had the highest number of PV neurons. In L5,

there significantly greater PV neurons in mouse V1 compared to monkey V1. There was significantly higher density of CR neurons in the upper middle layers of Monkey V1 compared to mouse V1 and monkey LPFC compared to mouse FC. The upper middle layers of monkey V1 had significantly higher density of PV neurons compared to monkey LPFC and mouse V1. There was significantly higher density of VGAT particles in monkey V1 and LPFC compared to mouse V1 and FC, which indicates more inhibitory synapses. There were significantly more VGAT+ boutons colocalized with PV+ boutons than CR+ boutons. Finally, discriminant analysis and hierarchical cluster analysis show that species is the largest separating factor between monkey V1, LPFC and mouse V1 and FC. Mouse V1 and FC are very similar, and monkey V1 and LPFC are dissimilar from one another. This data, united with comparative data on pyramidal neurons, demonstrates that neurons have differences between species, and monkeys have more regional specialization than mice.

TABLE OF CONTENTS

LIST OF TABLES

LIST OF FIGURES

LIST OF ABBREVIATIONS

CB.....Calbindin

CR..... Calretinin

DA ..... Discriminant Analysis

DAPI..... 4',6-diamino-2-phenylindole

FC ..... Frontal Cortex

FS ..... Fast Spiking

GABA.....Gamma Aminobutyric Acid

HCA..... Hierarchical Cluster Analysis

IN.....Interneuron

PFC.....Prefrontal Cortex

PV..... Parvalbumin

ROI .....Region of Interest

V1 .....Primary Visual Cortex

VGAT .....Vesicular GABA transporter

INTRODUCTION

Interneurons

Cortical interneurons (INs) gate excitatory signals by inhibiting pyramidal cells. Pyramidal neurons are the most populous of the excitatory neurons found in the cortex of most mammals. They are named for their pyramid shaped soma, and they have a short and wide arbor of basal dendrites and a longer cluster of apical dendrites. (Bekkers, 2011). INs inhibit pyramidal cells through the use of the neurotransmitter gamma aminobutyric acid (GABA) and GABA uptake is regulated by GABA transporters. Vesicular GABA transporter (VGAT) is involved with the uptake of GABA and its storage in synaptic vesicles (Gasnier, 2004). INs can form connections with pyramidal cells through mechanisms such as feedforward inhibition and lateral inhibition (Buzsáki, 84; Knowles & Schwartzkroin, 81). INs play an important role in establishing the spatio-temporal dynamics of neural circuits (Somogyi & Klausberger 05).

GABAergic INs are found in all cortical layers and display various morphological, molecular, and physiological characteristics. The structure of a cell often dictates its function. The targets of a cell's axons are hallmark features of cell classification. They can be divided largely into cells that target pyramidal cells, and those targeting other interneurons. INs can be further classified by postsynaptic targets such as: axons, somata, or dendrites of the postsynaptic neurons. Dendrite-targeting can also be subdivided into whether INs preferentially synapse on spines or shafts. These categories have distinct physiological characteristics that influence the cell's role in neural circuits. Unique peptide and protein markers, mainly calcium binding proteins, can be used to categorize INs. There

are many morphologies and protein markers that INs express, and they can also be classified into groups that share physiological attributes (Zaitsev et al., 2015). Physiological properties can often be inferred based off of the molecular properties of the cell. There are six main physiological types- “Fast-spiking (FS) neurons show non-adapting spiking at steady-state, brief spikes, and large fast after-hyperpolarizations and continuous FS cells, delayed FS cells, stuttering FS cells, and continuous stuttering FS cells” (DeFelipe et al., 13). The electrophysiological properties of a cell determine the effect of its input on the target cell. Parvalbumin cells provide strong inhibitory input onto pyramidal cells due to their fast non-adapting high amplitude electrical firing patterns and their proximity to the axon as they synapse on somata. All of these properties exist simultaneously on a cell, so a multi-dimensional perspective is crucial to properly identifying a cell, some of these properties are shown in Figure 1.

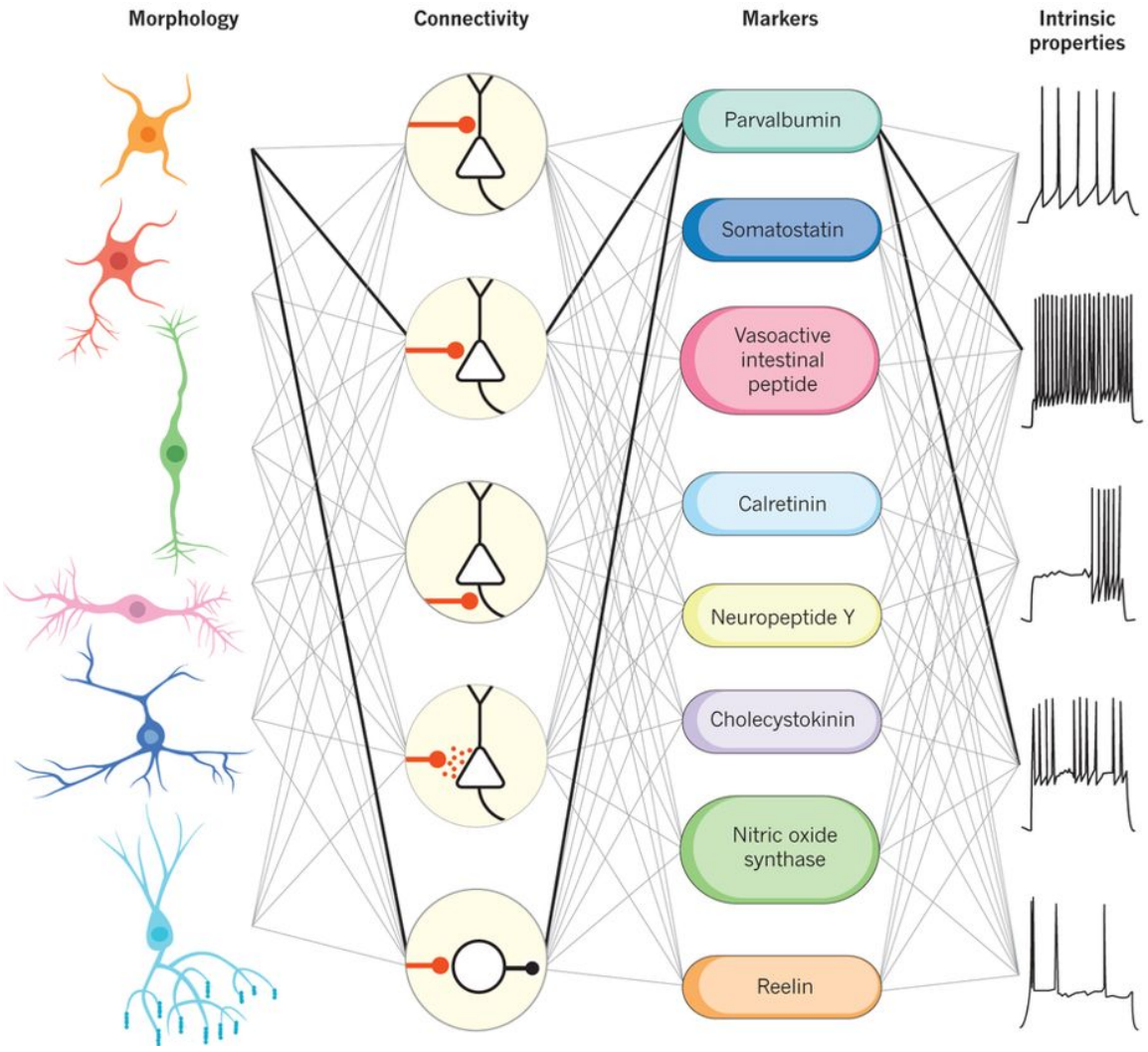

Figure 1: Multiple Variables Used for Classifying Interneurons: Highlights how INs can be defined through multiple parameters such as morphology, connectivity pattern, marker expression, and intrinsic properties. We used markers to initially categorize cells, then we used other methods, like cell reconstruction, to determine other qualities of the cells. Adapted from Kepeces & Fishell 2014

Parvalbumin (PV), Calretinin (CR), and Calbindin (CB) constitute majority of the calcium-binding proteins markers. Their receptors bind with Ca^{2+} with high affinity and they are thought to act as a buffer for Ca^{2+}. PV and CR form distinct categories and they rarely stain the same cell. PV neurons comprise 40% of all GABAergic neurons (Rudy et al., 2011). CR neurons account for about 14% of GABAergic cells (Tamamaki et al., 2003). Amongst several mammals including humans, rats, monkeys; and exotic mammals such as platypuses, chinchillas, and beluga whales, there are differences in the density and distribution of PV CR and CB. They can function as chemoarchitectonic markers for regional and laminar differences in mammals (Hof et. Al 1999).

CR neurons and PV neurons have particular distinctive morphologies. For example, based on morphology, most PV neurons are basket cells or chandelier cells. There is more diversity of CR neurons, but the most common morphologies are double bouquet, bipolar, and Cajal-Retzius cells (Defelipe 1997), as shown in Figure 2. The morphology of the cell also dictates the role of the cell in terms of circuit dynamics. The PV basket cells target mainly the somata of pyramidal cells, while PV chandelier cells mainly target axon initial segments of pyramidal cells (Deflipe 1997). A review from Barinka and Druga in 2010 integrated and summarized findings Gabbot and Colleagues' comprehensive survey of the morphology and distribution of CR neurons in rats (Gabbot et al., 1997) and monkeys (Gabbot and Bacon 1996a,b). There were significant similarities in morphology amongst species; however, the density was greater for CR neurons in the PFC of monkeys compared to rats.

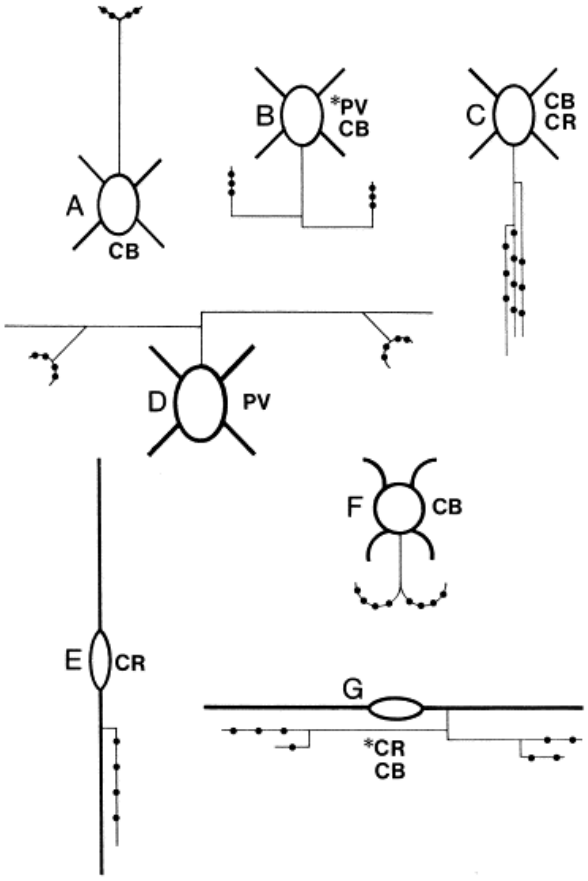

Figure 2: Common Morphologies of Neurons Expressing Calcium Binding Protein Markers:"Schematic drawing showing the main types of smooth non-pyramidal neurons and their content in the calcium-binding proteins calbindin (CB), parvalbumin (PV) and calretinin (CR) in the neocortex. Asterisks indicate the most common calcium-binding protein: (A) Martinotti cell; (B) chandelier cell; (C) double bouquet cell; (D) large basket cell; (E) bipolar cell; (F) neurogliaform cell; (G) Cajal–Retzius cell." Adapted from Defelipe 1997.

Parvalbumin positive basket cells are one of the main sources of inhibition onto pyramidal neurons. They come in two main morphological types, basket and chandelier cells. The axonal arbor of basket cells forms a "basket" around the soma of pyramidal cells and INs. They provide strong inhibition onto pyramidal cells and other INs through their fast and high amplitude inhibitory signals. PV neuronal inhibition is strongest at the soma and gets progressively weaker as it goes to the dendrites and spines. Their axonal arbor synapses onto multiple pyramidal neurons which allows PV neurons to exhibit global control over pyramidal neurons in a layer. (Kubota et al., 2015). Chandelier cells are axo-axonic neurons and best defined morphologically (DeFelipe et al., 2013). Basket cells predominantly target cells perisomatically which implies that they are generally involved in local inhibition, but PV cells can also inhibit cells in other layers with their axons that span across multiple layers. The largest concentration of PV neurons tends to be from lower layer 3 to upper layer 5 in monkey pre-frontal cortex (PFC) and rat mPFC (Gabbot and Bacon 1996, Gabbot et al., 1997). This is where the somata of long projecting pyramidal cells are located, which supports the function of PV neurons as strong inhibitors of pyramidal., Layers 2 and 3 in the mPFC of rats hold the highest density of PV puncta (Gabbot et al., 1997).

The post-synaptic targets of PV neurons are the somata, dendritic shafts, and spines of pyramidal neurons (DeFelipe et al., 1989). Synaptic targets of CR-containing cells are more heterogeneous and relatively less well characterized. In the primary visual cortex (V1) of primates, CR-containing cells form synapses with dendrites of other interneurons in superficial layers and inhibit pyramidal cells in deeper layers (Meskenaite 1997). In PFC

these neurons mainly form symmetric synapses onto dendritic shafts, dendritic spines, or somata. In deeper layers, there are more asymmetric synapses, which are glutamatergic. CR neurons have different synapses in different layers, suggesting that CR targets different cell types depending on the layer of cortex. (Melchitzky et al., 2005). This also suggests that CR neurons are more heterogeneous and play a variety of roles in circuitry. CR neurons can inhibit the dendrites of pyramidal neurons; CR neurons can also inhibit other interneurons which consequently can disinhibit pyramidal cells. CR neurons primarily target other interneurons. CR neurons can synapse onto PV neurons, which in turn target the somata of pyramidal cells. This is one mechanism for how CR neurons can disinhibit pyramidal cells (Gabbot et al., 1996).

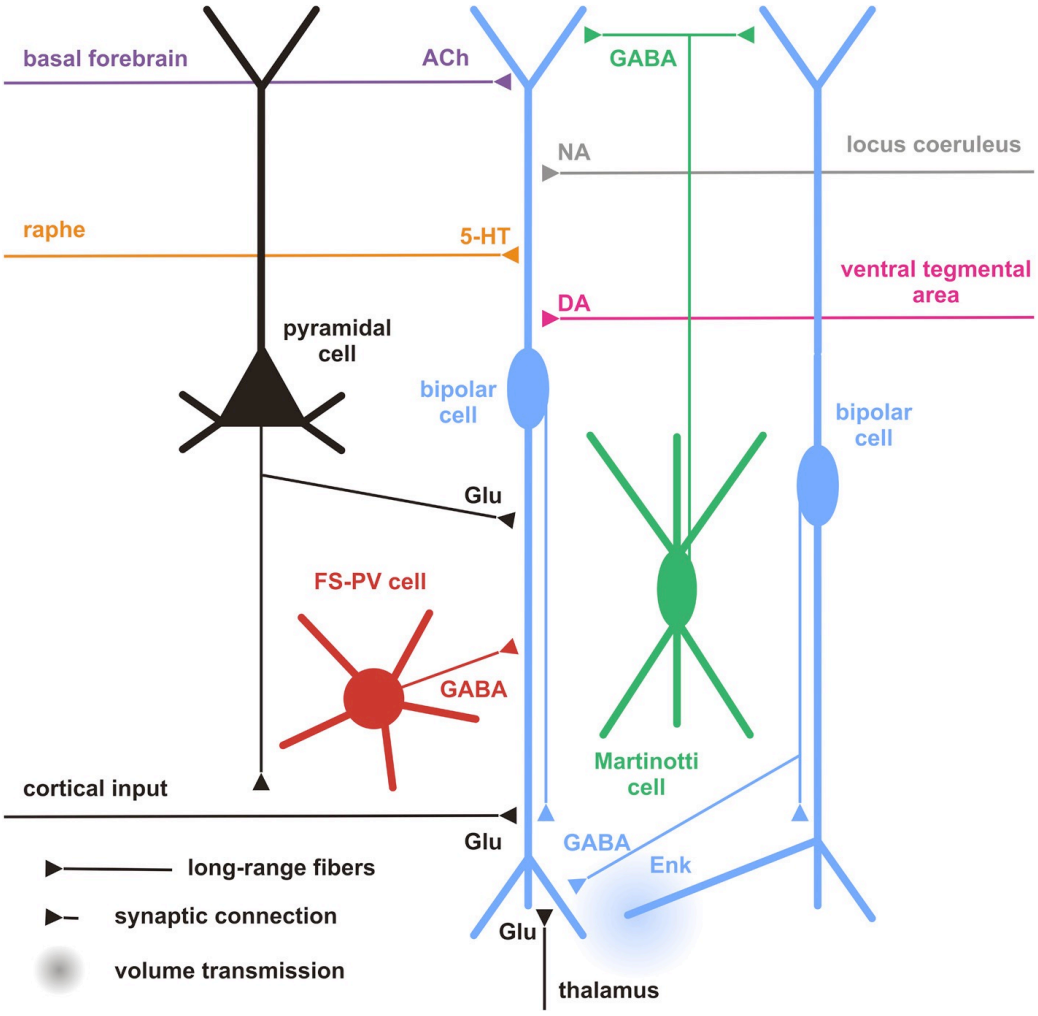

Figure 3: Neuronal inputs onto bipolar CR neurons. Somata are the round or oval shaped structures in the middle of the cells. Thick lines represent dendrites and thin lines represent axons. Adopted from Cauli et al. 2014

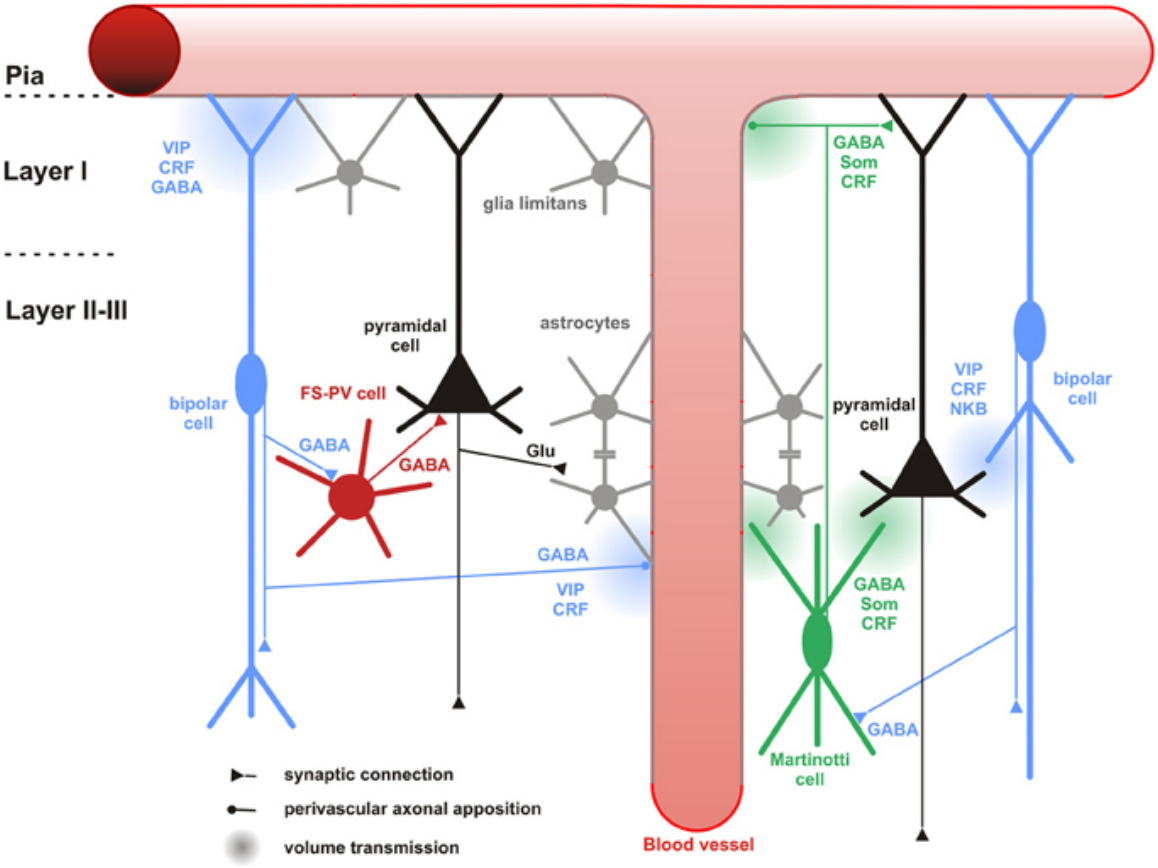

Figure 4: Neuronal outputs of bipolar CR neurons. Somata are the round or oval shaped structures in the middle of the cells. Thick lines represent dendrites and thin lines represent axons. Adopted from Cauli et al. 2014

CR neurons receive inputs from a variety of neurons and there are several potential targets for the synapses. Figure 3 shows the synaptic inputs onto bipolar CR neurons. Pyramidal cells target the dendrites proximal to the soma, which provide strong excitatory signals to CR neurons. Axon collaterals of deeper pyramidal cells and the terminal axons from long-distance projections of pyramidal cells in other brain areas can provide input onto CR neurons (Gabbot, 2016). PV cells provide strong inhibitory inputs onto proximal dendrites CR neurons also receive weak inhibitory inputs from other CR neurons in distal dendrites. Figure 4 shows the synaptic outputs of bipolar cells. These INs can synapse onto bipolar neurons on distal dendrites or onto the somata of PV cells to disinhibit pyramidal cells. And they can signal to pyramidal cells with volume transmission. Volume transmission is the signal diffusion of neurotransmitters and ions along the extracellular fluid (Agnati et al., 1995). CR and pyramidal cell dendrites are in close proximity, which allows volume transmission between the two cell types (Cauli et al., 2014).

Laminar Distribution of Interneurons

The neocortex has a unique function of integrating and analyzing information from the rest of the nervous system. It analyzes and manages internal and external environments. The cortex consists of neurons and glia generally stratified in a laminar pattern with 6 layers. The laminar distribution of neurons provides insight into the inputs and outputs of a neuron. When a neuron is said to be in a particular layer it is referring to its soma and proximal dendrites, yet for example, a neuron from layer 4 may have dendrites and axonal projections that span multiple layers.

The organization of cortical layers varies significantly across brain areas, but organizational patterns provide important insight into the role of a cell based on which layer the neuron resides. Figure 5 shows the laminar organization of neocortex. Layer 1 is the molecular layer, and "from the molecular layer downward these are the external granular (II), external pyramidal (III), internal granular (IV), and internal pyramidal (V) layers) (Grant, 2015). These layers are organized differently across species and brain areas. Laminar organization provides the framework for differences in cell population from different neocortical areas.

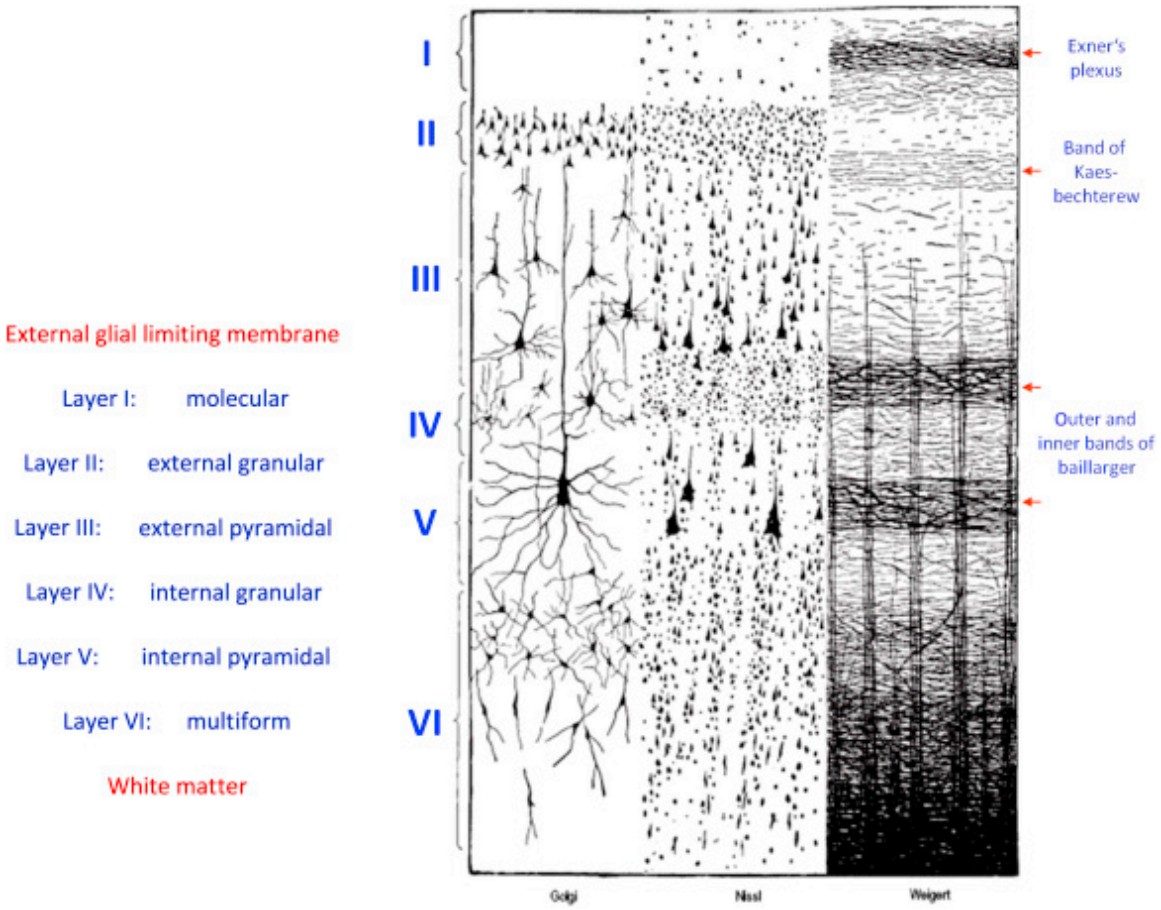

Figure 5: Laminar organization of neocortex. The columns represent different stains used to determine the columns. The names of the layers are based on the composition of the layers Adopted from Grant 2015

Layer 1 is closest to the pia and it is the outermost layer. All other layers run deep relative to layer 1. Layer 1 is called the molecular layer and has very few cell bodies. It consists mainly of axons running across the cortical surface, a few neurons and glia, and the apical dendrites of pyramidal cells in other layers (Grant, 2015). Layer 2/3 is referred to as the supragranular (above layer 4) pyramidal layers. It is also home to many basket cells, like parvalbumin cells, which provide direct inhibitory input onto pyramidal cells (Czeiger and White, 1997). Layer 4 receives dense inputs from the thalamus and accordingly is larger in primary sensory regions. Layer 5 contains the largest pyramidal neurons which project primarily to subcortical areas. Many long projecting fibers originate in Layer 6. Basket cells also reside here and they play an inhibitory role onto layer 6 neurons (Zhang and Deschenes, 1997).

Rodents (~16%) compared to primates (~24%) have a lower proportion of GABAergic neurons relative to the overall population of neurons. This is largely due to a threefold difference in the relative amount of CR neurons to total neurons in rodents (~4%) and primates (~12%). On the other hand, PV cells do not increase in proportion to the same extent as CR cells (Hladnik et al., 2014). In humans and monkeys, there are also twice as many CR cells in frontal and parietal regions. This suggests that they may play a role in higher-order associative and control functions (Dzaja et al., 2014). These conclusions show general interspecies differences in CR distribution, and more experiments are needed to understand the nuances of species differences in CR distribution.

The laminar distribution of cell types provides a spatial context for where groups of cells contact one another. PV neurons are found mainly in layers 2–4 which provide

strong inhibition to the pyramidal cells in those layers. CR neurons are mainly located in layers 1–3; this makes them conducive to targeting the dendrites of pyramidal neurons and other interneurons. Synapsing on different parts of the cell has different effects on the dynamics of the circuit. Layer 1 CR neurons receive inputs from excitatory neurons in L1, axon collaterals of deeper pyramidal cells, and terminal axons of long-projecting pyramidal cells in different brain regions (Gabbot, 2016). These CR neurons tend to have slow depolarization response which is due to the positioning of CR neurons onto the dendrites of other interneurons (Gonchar and Bulkhalter 2003).

Comparison between Species

Are animal models appropriate representations of human brains? 85% of animal research fails to lead to clinical interventions primarily because the research fails to ask the appropriate question and they fail to use the appropriate methods (Chalmers and Glasziou 09). This is especially a problem in neuroscience research, where for example there is yet to be a reliable and effective therapeutic to age-related cognitive decline. Two of the most commonly employed research subjects used to study brain structure and function are mice and non-human primates, specifically the rhesus monkey. Mice are a very practical research subject: they are inexpensive, readily accessible, reproduce quickly, and many of their genetic and molecular properties can be altered experimentally. The disadvantage of mice as a model is they can only perform a few complex behaviors and even those behaviors cannot be extrapolated to represent complex human behaviors. Monkeys have brains that are significantly more similar to humans, and they can perform tasks that are

substantially more complex than the ones mice can perform. Their disadvantage is that access to monkeys as research subjects is very limited, it is not ethically sound to employ large numbers of monkeys in research analogous to that performed in laboratory mice, they are expensive, and they have a much longer life span compared to mice.

Pyramidal cells have different characteristics in different brain regions of the monkey. Specifically, LPFC and V1 have different morphological and intrinsic properties. V1 pyramidal neurons are smaller with less robust dendritic arbor compared to LPFC (Gilman et al., 2017, Luebke, 2017). Morphological properties are sufficient to explain changes in passive properties. V1 pyramidal cells fire easier and faster (Amatrudo et al., 2012). Thus, in monkeys, there are observable differences in Layer 3 Pyramidal neurons between V1 and PFC, but there is not such a marked difference between the two areas in mice. Subtle detectable differences in dendritic morphology can affect the cable properties of dendrites and alter the signal processing capabilities of a pyramidal cell (Luebke, 2017).

Our lab has previously examined morphological, physiological, spine density, and ultrastructural synaptic differences of L3 pyramidal cells in monkey and mouse frontal and visual cortices. There is a scaling effect of dendritic size from mouse to monkey frontal cortices, while there is no scaling effect from mouse to monkey in V1. There are significant differences in the intrinsic membrane properties of Monkey V1 and LPFC, but there are no significant differences in mouse V1 and FC. Monkey V1 has lower density of spines compared to monkey LPFC and mouse V1 and frontal cortex (FC) (Gilman et al., 2017). There are more asymmetric synapses (excitatory) in mouse V1 and FC compared to monkey V1 and LPFC. There are significantly less asymmetric synapses in Monkey V1

and LPFC, but there are no significant differences between mouse V1 and FC. Taking into account the higher density of pyramidal cells in monkey V1, there are fewer synapses per neuron in monkey V1 compared to LPFC (Hsu et al., 2017). There are more VGAT appositions onto pyramidal cells and VGAT particles in monkey ACC compared to LPFC, indicating differences in inhibitory synapses between brain regions (Medalla et al. 2017). After a comprehensive analysis of pyramidal cells, the next step is to examine differences in INs across species and brain regions.

Prefrontal Cortex

The Prefrontal cortex (PFC) is one of the most studied areas of the brain due to its essential role in regulating acts of daily living and working memory. The PFC is involved in cognition, learning, executive function, and higher-order processing. It is implicated in diseases such as dementia, traumatic brain injury, major depressive disorder, autism, schizophrenia, attention deficit disorder, etc. (Fuster, 2008b). It is difficult to represent these complex behaviors appropriately in animal models. Modeling pathological states is also difficult considering the complexity and uniqueness of the human PFC. Understanding similarities and differences in the PFC between species is particularly important because it has been difficult to apply findings from animal studies to successful treatments in humans.

The PFC is a region of the brain located in the anterior pole. Most definitions of the human PFC contain Brodmann areas 8–13 and 44–47 (Fuster, 2008a). PFC can be defined by multiple parameters; nevertheless, it is an important area of study because it directs cognitive functions such as working memory and other complicated behavioral tasks

(Fuster, 2008b). There are discrepancies in an agreed-upon size and location of PFC across species. Some of this is due to methodological differences in studies. Some use different reference regions or species to determine what PFC is. “Generally, “PFC” is the frontal lobe association cortex anterior to motor and premotor regions.” (Donahue et al., 2018).

Comparison of brain regions between species is difficult due to a lack of standardized nomenclature for brain regions. This is particularly true for the PFC. Oftentimes regions are functionally defined by what behaviors they regulate. This creates different criteria for what is considered rodent PFC. Also, it is not automatically assumed that rats have a PFC. Early definitions were based on findings from Rose and Woosley (1948) which proposes that PFC should be defined as receiving inputs from the mediodorsal (MD) nucleus of the thalamus. Preuss (1995) claimed in a highly cited review that rodents are not useful models for certain prefrontal behaviors, but are useful for other areas such as cingulate and premotor cortices. There was a shift towards functional rather than structural definitions for PFC with the transition from positron emission tomography (PET) to functional magnetic resonance imaging (fMRI). There is some confusion when anatomical terms do not correspond with the same anatomical features across species. In rats, the PFC contains four main regions, medial, lateral, ventral, and orbital (Fuster 2008a). Generally, the PFC in rodents refers to medial frontal areas which correspond to the ACC in primates which is the agranular areas in the medial frontal cortex. Obvious size difference aside, primate brains are also considerably more curved i.e. concave front to back. This has significant implications on the differences in PFC between rodents and primates. Taking into account this curvature, the regions commonly associated with PFC

in rodents are rotated to correspond with ACC in monkeys (Laubach et al., 2018).

A comparative study found differences in PV basket cells in monkey and rat PFC. Monkey PV basket cells were easier to excite compared to the ones in mice (Povysheva et al., 2008). The basket cell horizontal spans were similar between species. The only difference between species was axonal length and axonal nodes. The differences in the firing properties of the basket cells between species could contribute to differences in gamma oscillation through synchronous, strong inhibitory signaling (Povysheva et al., 2008). There are also inter-areal differences in PV cell's physiological properties. We have also noted in previous experiments that differences in PV and CCK between ACC and LPFC of monkeys account for changes in the excitability and dynamic range of pyramidal cells. These factors influence gamma oscillations (Medalla et al., 2017).

FS-PV cells are phase-locked with pyramidal cells during gamma oscillations, and optogenetic studies indicate that they drive the gamma oscillations. They are sensitive to changes in sensory input and they gate excitatory output (Cardin et al. 2009). PV basket cell's morphology is conducive to synchronize signaling due to their wide dendritic arbor and electrical coupling with neighbors through gap junctions (Kawaguchi et al., 2019). These oscillations are involved in the PFC and executive control, the gamma frequency oscillations become desynchronized in pathological states such as schizophrenia (Gonzalez-Burgos 2015).

In the mPFC, as defined here (anterior cingulate cortex, prelimbic, infralimbic, motor cortex 2), bipolar CR neurons were mostly situated in layers 2 & 3 (Saffari et al., 2019). Multipolar cells were found primarily in layer 3 (Saffari et al., 2019). Their

physiological properties differ; all multipolar were adapting spiking, and all bipolar were fast-spiking. Layer 3 had the longest bipolar cells which can affect pyramidal cells in layer 5 (Saffari et al., 2019). This is important for feedforward inhibition because CR bipolar cells travel long distances to disinhibit INs across multiple layers. This impacts neurons that project to other regions of cortex, which is integral to the associative functions of the PFC.

Layers 2 and 3 have primarily 2 types of CR neurons: bipolar and multipolar. An experiment elucidated physiological properties of these 2 types of CR neurons. this categorization using genetically modified mice to express a sequence for EGFP located next to the CR gene (Saffari et al., 2019). Biocytin-filled cells and patch-clamp recordings were used to identify the functional properties of the cells. Bipolar CR neurons have long axonal projections that can extend to L5 pyramidal cells. Bipolar CR neurons are often electrically coupled with gap junction when they are close to each other. Whereas, Multipolar CR neurons are coupled with basket cells. (Saffari et al., 2019)

Primary Visual Cortex

V1 is the area that visual information first is encoded in the neocortex and hence it is often referred to as primary visual cortex. It is a good region for comparison in our study because there is extensive foundational research in V1 and it is relatively more straightforward (compared to PFC) to draw conclusions about cross-species similarities and differences within V1. There are some discrepancies for establishing species homologs of V1, but it is generally accepted that V1 is located in the occipital region of a phylogenetically conserved cortical sheet with a single laterally adjacent region, V2, which

is also conserved among mammals (Laramee & Boire 2015). V1 or Brodmann's area 17 occupies a substantial portion of the occipital pole. The medial surface of V1 is not as expansive along its dorsoventral length, but V1 continues along the banks of the calcarine sulcus. Hässler's (1967) laminar scheme for V1 is relatively consistent amongst primates. This is helpful for comparison with non-primate species because the distinct laminae allow for more accurate comparisons. Most experts will agree with the 6 distinct layers in V1 proposed by Hässler, but there are disagreements about defining layer 4 subdivisions.

The role that PV neurons play in neural circuits in vivo reflects the morphological predictions of PV's function. PV cells mainly target the somata and proximal dendrites of pyramidal neurons, and FS basket cells, the most common type of PV cells, exert strong inhibitory signals onto pyramidal cells. Optogenetic studies confirmed this phenomenon in mice; for example, mild to moderate photostimulation of PV+ cells gate pyramidal cells (Ingram et al., 2019). Varying morphological properties, such as the wide dendritic arborization of some PV neurons are conducive to their role in lateral inhibition (Kisvárday et al., 2002). Considering their relationship with pyramidal cells, it is no surprise that the response specificity of PV basket cells is reflective of the response specificity of their neighboring pyramidal cells (Runyan et al., 2010). The morphological variants of PV neurons in V1 form relationships with other cells that are conducive to the encoding of visual information. Temporal gating of visual stimuli is important to encode changes in visual space, such as movement. We should expect to see more PV neurons in V1 because of the abundance of PV neurons required for lateral inhibition of L4 pyramidal cells.

In monkeys 14% of long-distance projecting GABAergic neurons are CR and none

were PV+ (Tomioka and Rockland 2007). We can infer that the morphological differences between CR and PV neurons account for this. PV cells can have wide dendritic arbors, but they rarely project to other layers. Bipolar CR neurons are long and exist in multiple layers making them appropriate for long-distance signaling. We can see differences across species and brain regions. We need not look any further than V2 to see a difference in the distribution of CR double-bouquet cells and PV chandelier cells. There are significantly more PV chandelier cell terminals in V2 compared to V1. There are also few CR double-bouquet cells in V2 and none in V1 (DeFelipe et al., 1999). Both studies have varying methodologies, so it is difficult to draw definitive conclusions. This is a common problem with cross-species comparisons, which is why our experiment is valuable.

This project focuses on 2 populations of INs in 2 brain regions of mice and monkeys. Most comparisons of INs between rodents and primates are post-hoc comparisons from different studies, very few studies have compared rodents and primates simultaneously applying the same methodology to both species. This project examines the density, distribution, and VGAT particles across species and brain regions. This project was completed in conjunction with Louis Park who examined the morphology of CR neurons. Our experiments can be used to improve our models of excitatory:inhibitory neural circuits in diverse neocortical areas. Dendritic topology determines the signal processing capabilities of a neuron. The density and distribution of CR and PV neurons are indicative of inhibition at the population level. The laminar distribution of INs determines what inputs and outputs they receive, which affects local and long-distance circuit dynamics. CR neurons are mainly located in L2/3, so they have strong interactions with

L2/3 pyramidal cells. Based on the lower density of spines in monkey V1 pyramidal neurons, we should expect to see differences between species, but less so between brain areas (Gilman et al., 2017). We should expect to see differences in the density of inhibitory synapses by examining the amount of VGAT particles.

METHODS

Experimental Subject

The tissue was from animals that were sacrificed for previous experiments. Tissue was collected according to procedures approved by the Institutional Animal Care and Use Committee (IACUC) of Boston University School of Medicine. Table 1 contains information about each subject information. WT C57BL/6 mice were housed and kept in a 12h light/dark cycle before individual brain harvest in Boston University School of Medicine. All monkeys were young rhesus monkeys that were part of the larger project in an aging and cognition study as a control group subject. They were perfused in 4% paraformaldehyde. Initially, we used mice that were perfused with K glutaraldehyde because they were used in experiments involving electron microscopy. The mice tissue did not stain well for parvalbumin, so we switched to mice perfused using 4% paraformaldehyde. We used dLPFC and V1 tissue from 3 monkeys. We collected 3 slices from each animal and each brain region. The mice perfused using glutaraldehyde were mouse. We collected 3 slices from each animal and for each brain region. The mice we used for the experiment were from mouse. For the frontal region, we collected 2 slices from 2 of the mice. And we collected 3 slices 2 of the mice. We had to add an additional animal for the frontal region because we one slice was torn. We collected 3 slices from 3 mice for V1. This information is summarized in flowchart 1.

Table 1: Monkey experimental subject information. Shows the code, sex, age, and cohort of the monkeys used in our experiments

Monkey Code	Sex	Age	Cohort
AM311c	M	20 years	Middle aged, curcumin control
AM342c	F	19.2 years	Middle aged, curcumin control
AM350c	F	17.3 years	Middle aged, curcumin control

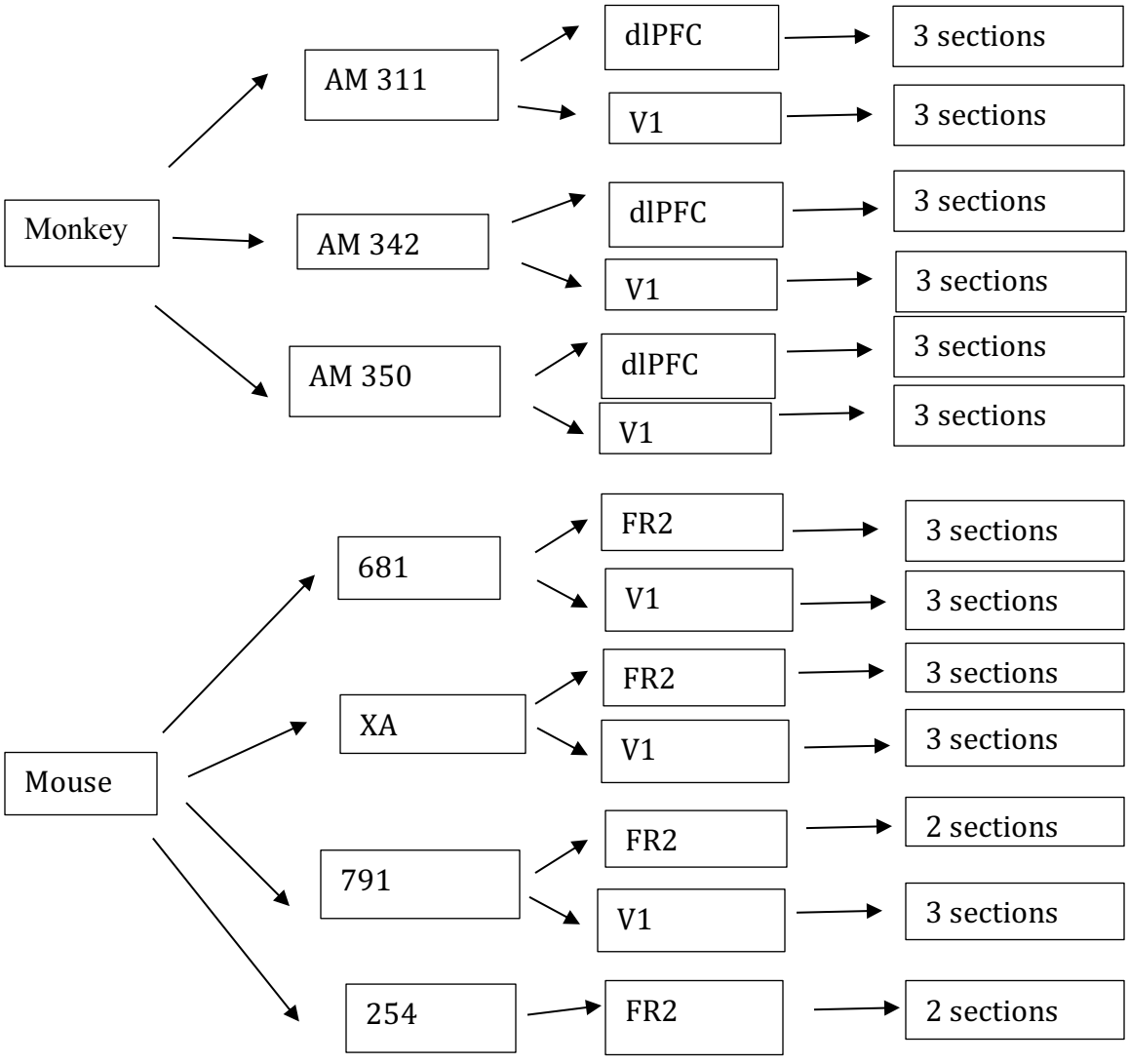

Figure 6: Flowchart of the tissue collected. The flowchart represents the serial sections collected from each animal in each region of interest (ROI).

Tissue Harvesting and Slice Preparation

Mice were anesthetized with ketamine hydrochloride (10mg/ml). 3 mouse brains were perfused by transcardial perfusion with 4% paraformaldehyde. 100μm coronal brain slices were prepared with the vibratome (Leica VT1000s) and cryo-protected to prevent denaturation of the tissue. Monkeys were perfused with ice-cold Krebs-Heinselt buffer (Sigma-Aldrich). Dura was quickly severed to expose the brain during perfusion. A block of tissue (10mm^3) were taken from LPFC and V1. Tissues were cut into 100μm slice while submerged in ice-cold oxygenated ringer solutions (concentrations, in mM, 26 NaHCO_3, 124 NaCl, 2 KCl, 3 KH_2PO_4, 10 Glucose, 1.3 $MgCl_2$; pH = 7.4, chemicals from Sigma).

Region of interest and tissue preparation

We retrieved tissue from Brodmann area 46 in the young Rhesus monkey. There is considerable debate about what is the homologous region to PFC in rodent cortex. Based on the reasoning discussed in the introduction, we selected the Fr2 area of rodent cortex to analyze. We retrieved tissue from monkey V1, Brodmann area 17. We also collected from V1 in the mice. We used the Allen brain atlas to locate the region of interest in the mice.

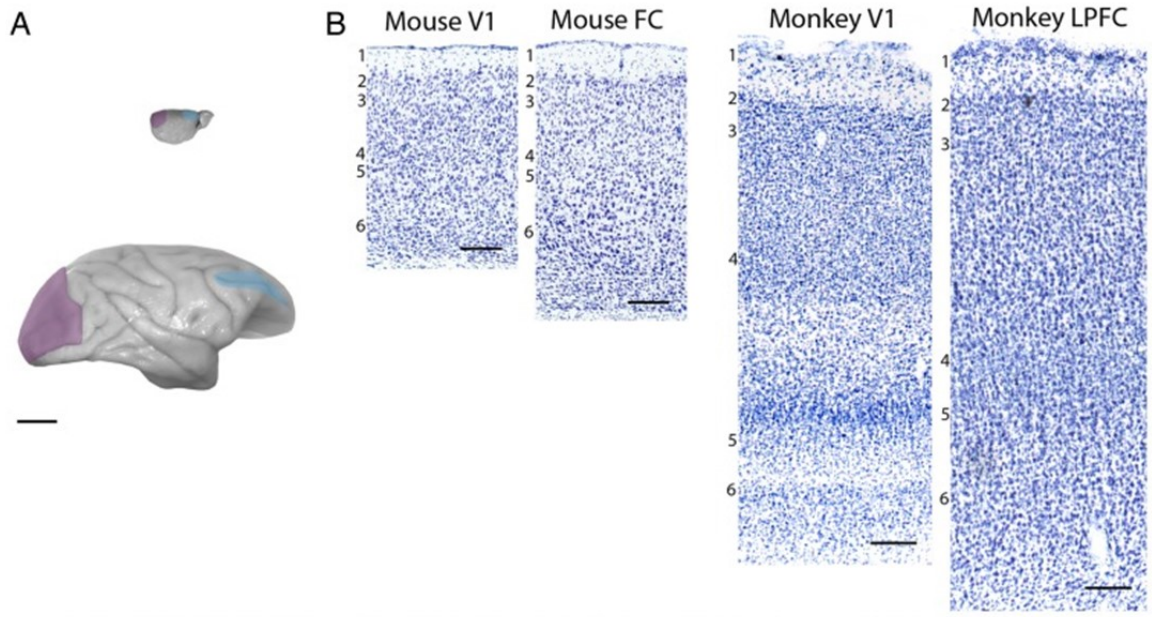

Figure 7: Regions of Interests. A) whole mouse brain (up) with FC (blue) and V1 (purple) B) whole monkey brain (up) with FC (blue) and V1 (purple). Scale bar is 1cm. B) Nissil-stained coronal sections of ROI. Scale bar is 200μm. Figure images and descriptions are adapted from Gilman et al., 2017

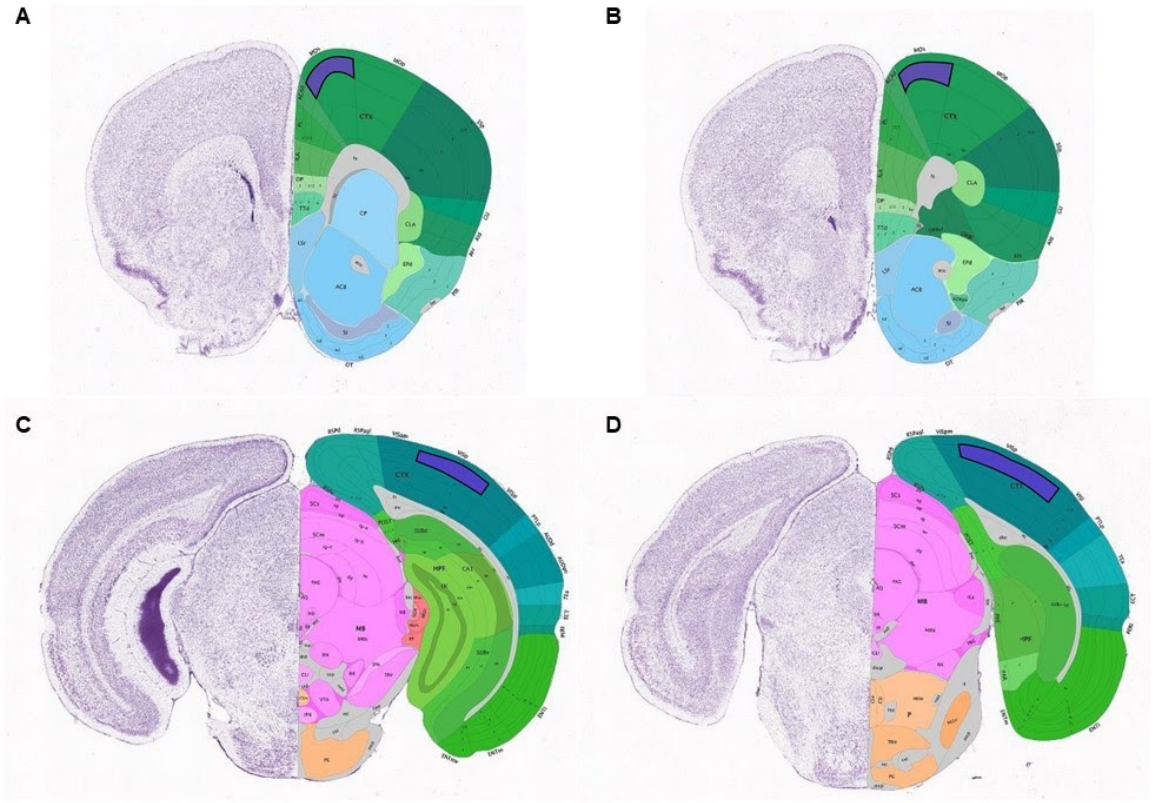

Figure 8: Regions of interest in the mouse brain viewed in coronal sections. A) Purple highlighted region indicates rostral end of the mouse premotor area, secondary motor cortex layer 2/3. B) caudal end of mouse premotor area layer 2/3. C) purple highlighted region is the rostral end of mouse V1 layer 2/3. D) caudal end of mouse V1 layer 2/3. Adopted from Allen Brain Atlas

Immunohistochemistry

On the first day, the tissue was first washed in 0.01M Phosphate-buffer saline (PBS) 4°C twice for 10 minutes each. The tissue was incubated in 50mM glycine in 0.01M PBS at room temperature for 1 hour. The tissue was subsequently washed in 0.01M PBS 4°C twice for 10 minutes each. Antigen retrieval was performed by incubating the tissue in a hot 10mM sodium citrate buffer while the culture plate rested in a water bath heated to 60–70°C. The tissue was subsequently rinsed three times 10 minutes each in 0.01M PBS at 4°C. The tissue was then incubated in for 1 hour in preblock solution using a solution of 0.01M PBS, 5% bovine serum albumin (BSA), 5% normal donkey serum (NDS), 0.1% triton-x (Tx), and 4 drops of mouse on mouse (MOM) block (Vector Laboratories inc, BMK-2022). The tissue was incubated in mouse anti PV (Swant, 1:1000), rabbit anti CR (Swant, 1:2000), and guinea pig anti VGAT (Synaptic Systems, 1:400). The monkey tissue was incubated in Rabbit anti CR (Swant, 1:2000), Goat Anti PV (Swant, 1:2000), guinea pig anti Vgat (Synaptic systems, 1:400) primary antibodies. The tissue was microwaved twice for 10 minutes using a PELCO Biowave pro plus at 150 MW for 10 minutes at 40°C. The tissue was incubated overnight for about 24 hours. On day 2, first the tissue was washed 3 times for 10 minutes in 0.01M PBS. Then, they were incubated in donkey anti mouse-Alexa 488, donkey anti rabbit-Alexa 546, and donkey anti guinea pig-Alexa 647. They were rinsed twice for 1 minutes in 0.1M PBS and once in .1 phosphate buffer (PB). The tissue was mounted and coverslipped with DAPI(4′,6-diamidino-2-phenylindole). All nuclei were stained by DAPI. Finally, the tissue was cured in the dark for 3 days, and then stored at 4°C.

Confocal Microscopy

The slides were imaged using a Leica TCS SPE microscope. Images acquired at 20x were for quantitative assessment of number of CR neurons. To capture a wide field, the 20x scans were done using the tile scan function on the microscope. The auto-stitching function on the Leica software leaves a 10% overlap. When stitched together it can cause slight shifts between adjacent tiles but cells that span across 2 tiles were still easily identifiable. The slight shift in the tiles while stitching during the tile scan function is not acceptable for reconstructions because the dendrites have to be continuous. Images acquired at 40x were used for reconstruction. To maintain the integrity of image while stitching the tiles, each tile was individually scanned and stitched together in Neurolucida. The 20x images had a voxel size of 0.538x0.538x1 and 1.5 numerical aperture in water immersion. The 40x images had a voxel size of 0.0896 x 0.0896 x 0.3 and 1.3 numerical aperture in oil immersion. The images were deconvolved in the Autoquant software to eliminate scattering of light from the media and the slide.

Confocal images taken from coronal sections stained for CR and PV of monkey LPFC and V1, as well as mouse FC and V1. Figure 9 shows deconvolved 20x images of the brain regions used for counting neurons. For monkey LPFC and V1, a column from the pia to white matter about 800 μm wide was imaged and counted from each section. A total of 3 sections were sampled, amounting to an average of $2.4*10^8$ μm^3 volume sampled in LPFC and $3.6*10^8 \mu m^3$ volume sampled in V1 from each animal (Fig 9A, B). For mouse areas FC and V1, images were acquired encompassing the entire gyrus (Fig 9C, D). For mouse FC, cell counts were obtained from area FA in the dorsomedial aspect, from 3 serial

sections, totalling to an average of $1.5*10^8 \mu m^3$ volume sampled from each animal. Images of FC include Infralimbic and prelimbic regions, but these areas were not counted for this study. The area that was counted totaled to an average of $6.8*10^7$ μm^3. For mouse V1 cell counts were obtained from coronal sections of V1, from 3 serial sections totalling to $6.3*10^8$ μm^3. White matter and parts of the hippocampus were included in some sections, and we counted from an average of 80.6% of the total volume imaged. For each animal, an average of $5.1*10^8$ μm^3 was used to count PV and CR neurons.

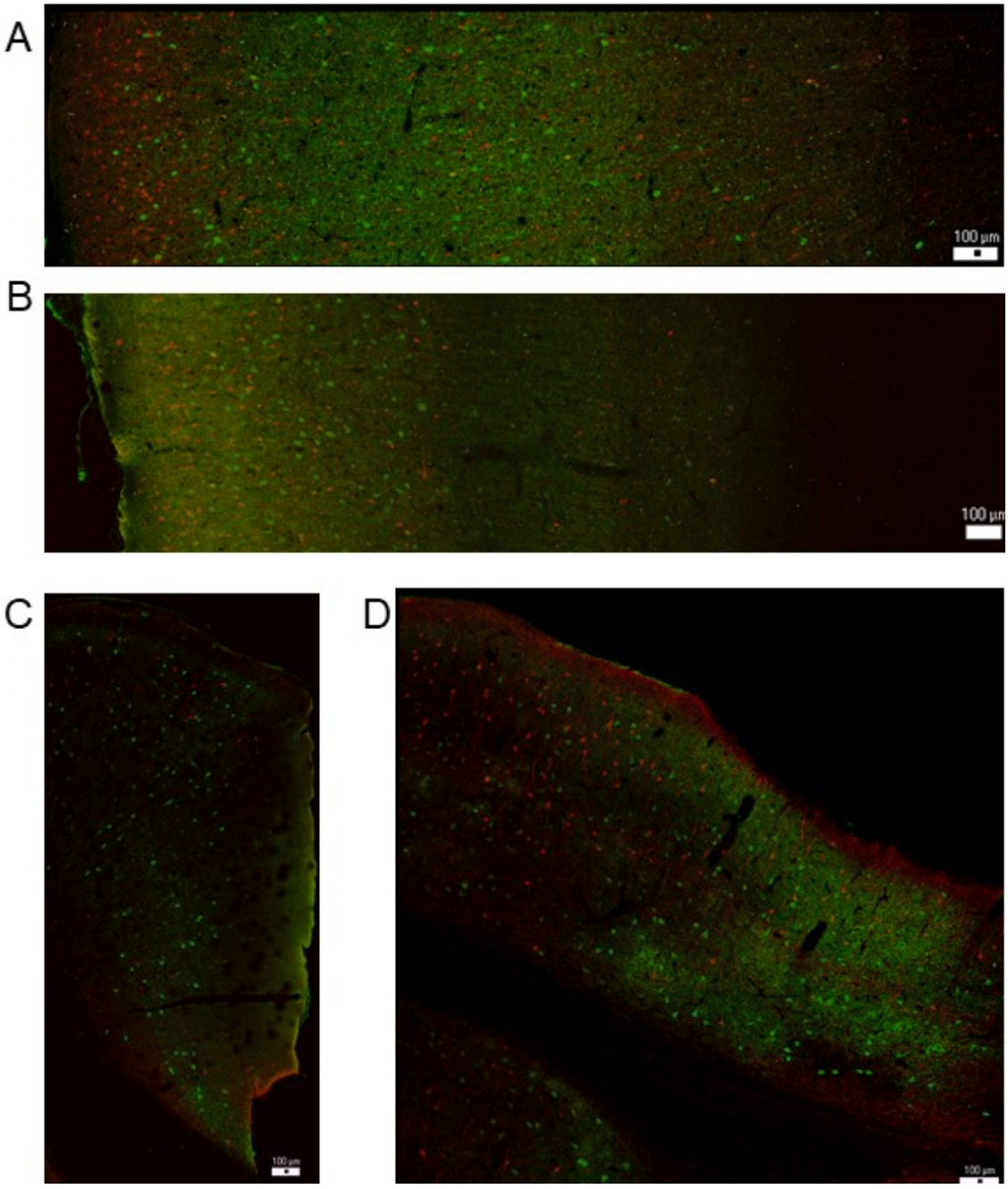

Figure 9: 20x confocal images used for counting neurons A) monkey LPFC immunostained tissue labeled PV and CR antibodies. Pia is to the right and white matter is to the left. CR is red and PV is green for all images. B) monkey LPFC immunostained tissue labeled PV and CR antibodies. Pia is to the right and white matter is to the left. C) Mouse FC immunostained tissue labeled PV and CR Antibodies. Pia is on the left and top of the image. The white matter is deep in the tissue. D) Mouse V1 immunostained tissue labeled with PV and CR antibodies. The Pia is on the top right and the white matter is the area with significantly less immunolabeling near the bottom left corner.

Quantification of number of CR and PV neurons

The 20x images were opened in the Neurolucida version 2019. Figure 10 shows the process of quantifying the number of neurons from the confocal images of monkey and mouse slices. The images from Figure 10 are taken from the same slice with contours and markers from Neurolucida superimposed onto the images. Figure 10A shows a deconvolved image of monkey LPFC tissue. The inset in the upper layers, is shown in higher magnification to show the somata that were counted. The density of CR is relatively high in this area. The marked contours are shown in Figure 10B. The L1-3 and L4-6 contours were used to determine the density of CR neurons. This demarcation was chosen based upon distances from pia . Pia and white matter contours were used to calculate the distances of individual neurons from said structures. Incomplete cells were discounted at the edge of 3 orthogonal planes i.e. top/bottom, right/left, superficial/deep. Moving through the stack, markers were placed on distinct cells. Their somata had to have a clear outline. If it appeared that 2 soma's overlapped, then 2 markers were placed. The markers were placed as close to the center of the cell as possible. Both CR and PV cells were counted. In one field, all of the neurons for both groups were be counted before moving to the next field. Markers were applied on cells throughout the entire stack, then counted in the same manner in an adjacent tile.

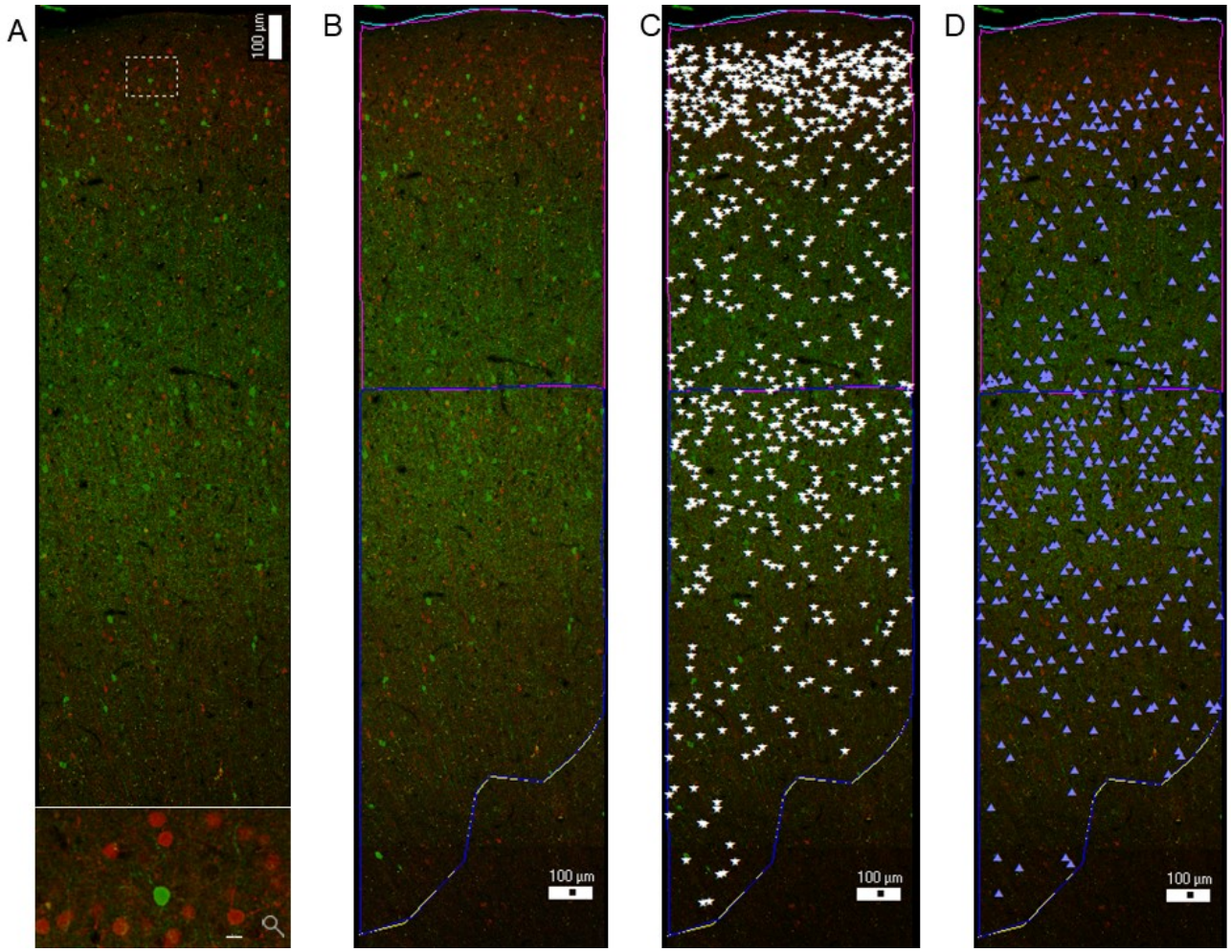

Figure 10: Process of counting neurons A) monkey LPFC immunostained tissue with PV and CR. Pia is towards the top of the panel. The inset in the upper layers is magnified to show individual somata. The scale bar for the magnified portion is 10µm. B) includes a pia (light blue), white matter (yellow), Layers 1–3 (pink), Layers 4–6 (dark blue). C) includes markers for CR (white stars) D) includes markers for PV (dark blue triangles)

Each marker had a 3D coordinate associated with it and this was used to calculate the distances from soma to pia and white matter. The distances were to an open contour drawn on the software representing the pia and the white matter. The distances to the pia and white matter are used in the distance calculations. Layers were determined based on consensus in the literature for the % depths of each of the layers. We attempted to corroborate the findings in the literature with the experimental observations using the DAPI staining. We overlaid the DAPI images with the images acquired from the confocal microscope to determine the layers based on the amount of granulation of nuclei. The DAPI stain did not work because making a montage of the DAPI images is difficult due to the quality of the images and lack of distinguishing figures required to overlap fields for montage.

Instead, the layers were binned based off on previously used laminar boundaries in the literature. The layers were binned as a proportion of the total thickness of the cortex for each area (Table 2). For monkey LPFC and V1, layer boundaries were based on Pierri et al. 1999. The layer boundaries for mouse V1 were based on boundaries used in Xu et al. 2016. The layers for mouse Fr2 were extrapolated from the layer boundaries for the prelimbic region used in Anastasiades et al., 2018. It was an The extrapolation of mouse Fr2 laminar distances from prelimbic regions was appropriate because these two regions are adjacent to one another, so differences in the boundaries of the layers are negligible.

Table 2: Layers determined for each group based on percent distance from pia.

	Monkey V1 and LPFC from Pierri et al. 1999	Mouse V1 from Xu et al. 2016	Mouse prelimbic from Anastasiades et al. 2018
L1	0–10%	15%	12.5%
L2/3	10–35%	15–40%	12.5–32.5.5%
L4	35–60%	40–50%	35–40%
L5	60–80%	50–75%	40–65%
L6	80–100%	75–100%	65–100%

Particle Analysis and Colocalization

Confocal image stacks of 100µm thick sections were labeled for VGAT, PV and CR (40x/1.3 NA, oil—immersion; 0.00896 0.00896 0.3m voxel) containing neuropil from L2-3 of monkey LPFC, V1 and mouse FC and V1. A sub-stack of 50 slices was used for particle analysis. The sub-stacks were created starting from slice 0, unless there was a problem with surface background. In those cases, the sub-stacks initiated when the background disappeared, and the sub-stack criteria was applied to the entire animal and brain region. The density of VGAT particles was analyzed using the particle analysis function of ImageJ (RRID:SCR_003070; Schneider et al., 2012). Particle analysis quantified the number of labeled puncta and the fractional covered area. ImageJ EzColocalization plug-in was used to assess VGAT puncta on CR and PV processes.

Statistics

All data were exported to Microsoft Excel spreadsheets using Neurolucida Explorer (MBF Bioscience). T-tests were conducted in Microsoft Excel. ANOVAs were conducted in SPSS (v24 IBM Company). Post hoc tests were conducted in MATLAB. Significance was set at $\alpha = 0.05$ for all statistical tests. Correlations were expressed as a Pearson product–moment correlation. Two tailed t-tests for each bin was conducted for the comparisons of neuronal distance. There are differences in cortical thickness between species and brain region, so we could not conduct a repeated measures test. The significance values for all data are reported in tables 3 and 4. One-way repeated measures ANOVAs with Bonferroni post hoc tests was attempted for the percent distance from pia analyses. The *n* was too low to be able to see the interaction of species, brain region, and percent distance from pia. Instead, one-way ANOVAs with Bonferroni post hoc tests were conducted for each of the bins. The significances are reported in tables 5 and 6. A 2-way repeated measures ANOVA was conducted for each laminar analysis with the dependent variables of species with 2 levels, V1 and frontal cortices, and layer.

For the density of CR and PV neurons we used 2 separate 2 way ANOVAs. Based on exploratory data analysis including a principle component analysis, we separated the IN type variable because they were distinct enough to be analyzed separately. We had 4 factors, monkey LPFC, monkey V1, mouse FC, and mouse V1. Each factor had 2 levels, layers 1–3 and layers 4–6. The residuals were not normally distributed for the CR ANOVA and this was confirmed with the Q-Q plot. A log transformation showed normally distributed residuals, satisfying the requirements to conduct the ANOVA. PV also had

residuals that were not normally distributed. The Q-Q plot verified that finding. A log transformation showed normally distributed residuals, satisfying the requirements to conduct the 2-way ANOVA. A Bonferroni post hoc test was conducted if the interactions were significant.

Discriminant analysis (DA) and hierarchical cluster analysis (HCA) were performed to assess the clustering of species and brain region. The stepwise DA was conducted to identify which factors created the most between group variability. A canonical correlation, r and Wilks' λ were used to measure the goodness of fit and significance of group discrimination. HCA groups areas based on (dis)similarities in their factors which are expressed as Euclidian distances, the result is a cluster tree diagram. The distances between 2 branches represents the similarity i.e. the longer the distance the more dissimilar are the groups.

RESULTS

Inter-areal comparison of the distribution of CR and PV neurons

The distance from pia of individual neurons was measured and binned to plot a distribution of neurons as a function of cortical depth. The significant differences between species and area within each bin are summarized in tables 2 and 3. The markers are heterogeneously distributed across layer based on area and species. (Fig. 11A, B). CR in monkey has the least inter-areal differences, monkey V1 has significantly greater number of CR at 50–150μm compared to monkey LPFC($P<0.05$) (Fig. 11C). Monkey LPFC and V1 follow the same pattern of having a high-density region in the first 500μm, and a slightly less dense region from 750–1000μm with subsequent tapering. There are more noticeable inter-areal differences of CR neurons in mice. There are significantly greater number of CR neurons in mouse V1 compared to FC from 100–800μm ($P<0.01$), but they follow a similar pattern of a high concentration close to the pia of CR neurons followed by a sharp decline, then a slight plateau followed by a small decline (Fig. 11D). In mouse FC, the bump and plateau occur at a shorter distance from pia compared to mouse V1. This can be attributed to gross anatomical differences between mouse FC and V1 (Laubach et al. 2018).

There are more regions of significant inter-areal difference in PV neuronal distribution than in the distribution of CR neurons. In LPFC, there is a slight dip in the density of PV neurons from 250–750μm followed by a relatively large increase from 750 μm to 1000 μm, then a decrease. Monkey V1 has a large increase in the first 750μm followed by a plateau from 750 μm to 1000 μm then a decline. The number of PV neurons

is a significantly higher in V1 from 100–700μm compared to LPFC ($P<0.01$), the region of the peak in PV density (Fig. 11E). In mice, V1 has more PV neurons compared to FC from 100–800μm ($P<0.05$). There is also a clear peak in PV neurons at 400μm in mouse V1. On the other hand, PV in FC increases slightly then plateaus for the majority of the depth of the tissue (Fig. 11F). While mice have more stark differences in inter-areal neuronal distribution, monkeys have subtler differences in the laminar distribution of CR and PV neurons, particularly PV. The only significant inter-areal difference in CR neurons in monkey occurs at 50–150μm, which is before the largest number of PV neurons in V1. This gives evidence to laminar separation of PV and CR neurons.

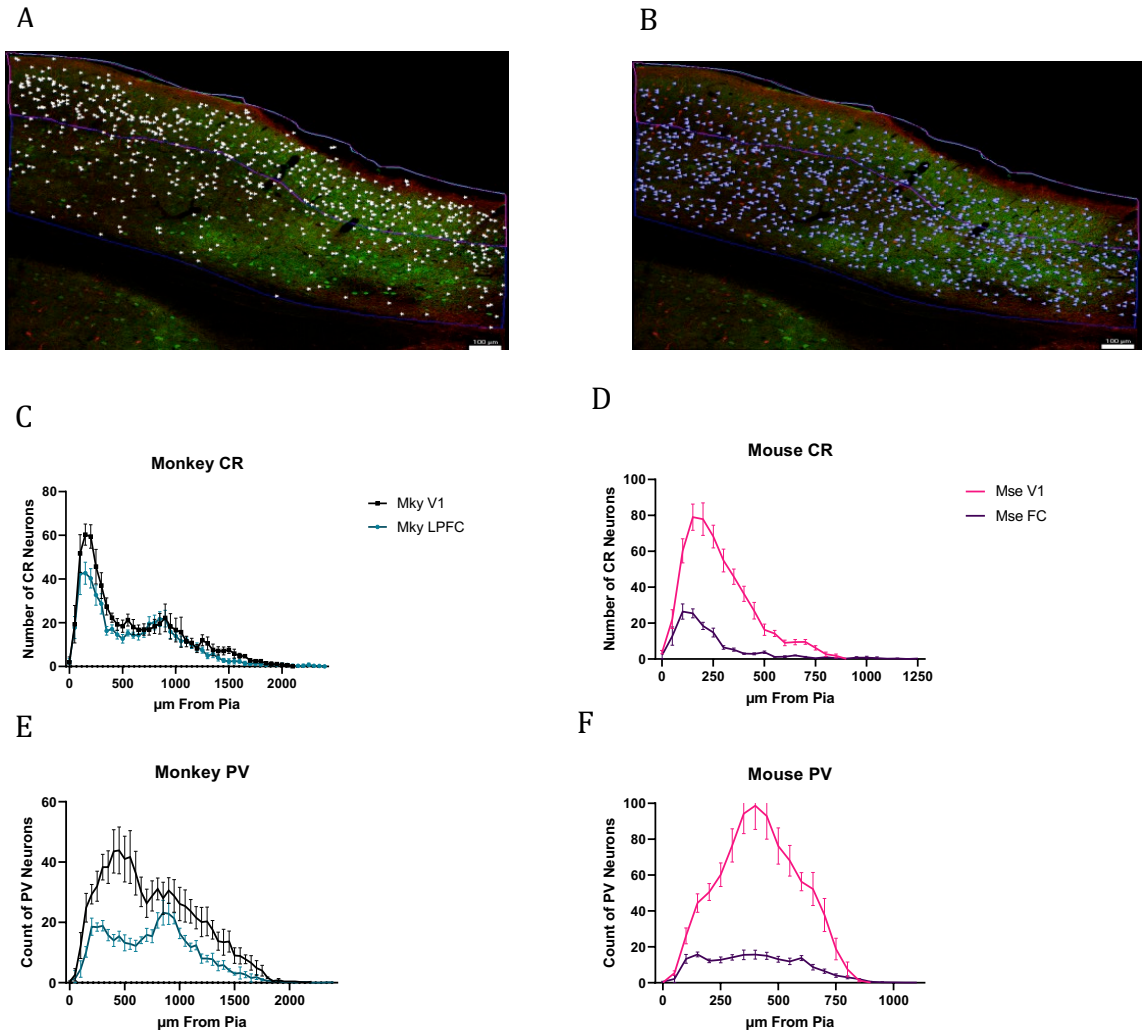

Figure 11: Inter-areal differences of CR and PV in monkey and mice. A) Mouse V1 immunostained tissue with CR markers. B) Mouse V1 immunostained tissue with PV markers. C–F) Comparing the counts of CR and PV neurons between brain areas. The bins are 50µm.

Inter-species comparison of the distribution of CR and PV neurons

The distribution of CR and PV neurons was compared between monkey and mouse cohorts (Fig. 12). The cortical depths are thinner in the mouse than the monkey. The results for the T-tests for the bins are found in tables 2 and 3. In both species, there is a peak in concentration of CR neurons at a depth of 250µm of V1 (Fig. 12A). However, there are significantly more CR neurons in Mouse V1 from 100–650µm, compared to monkey V1 ($P<0.05$). Depth does not extend past 1000 µm in mouse V1, but it does in monkey V1. In contrast, monkey LPFC has significantly more CR neurons than mouse FC throughout upper to deep layers, from 100–1100µm from the pia ($P<0.05$, Fig. 12B). Monkey LPFC has its greatest peak in CR concentration at 250 um then it has another smaller peak from 750–1000µm (Fig. 12B).

Monkey and mouse V1 have different patterns of PV distribution (Fig. 12C). Mouse V1 has an incrase and decrease of PV that forms a sharp peak at ~450µm. Monkey V1 has a gradual increase to a peak at ~450µm followed by a more gradual decline. Compared to monkey, mouse V1 has significantly more PV neurons from 150–450µm ($P<0.05$), 550–750µm ($P<0.05$), and 750–900µm ($P<0.01$). Monkey LPFC and mouse FC have no significant differences in PV neuronal count for the first 600µm, except from 200–350µm ($P<0.05$). Monkey LPFC has a significantly higher PV neuronal count from 650–900µm ($P<0.05$). While mouse V1 has more CR and PV neurons in comparison to monkey V1, this difference is more pronounced in PV neuronal count (Fig. 12D).

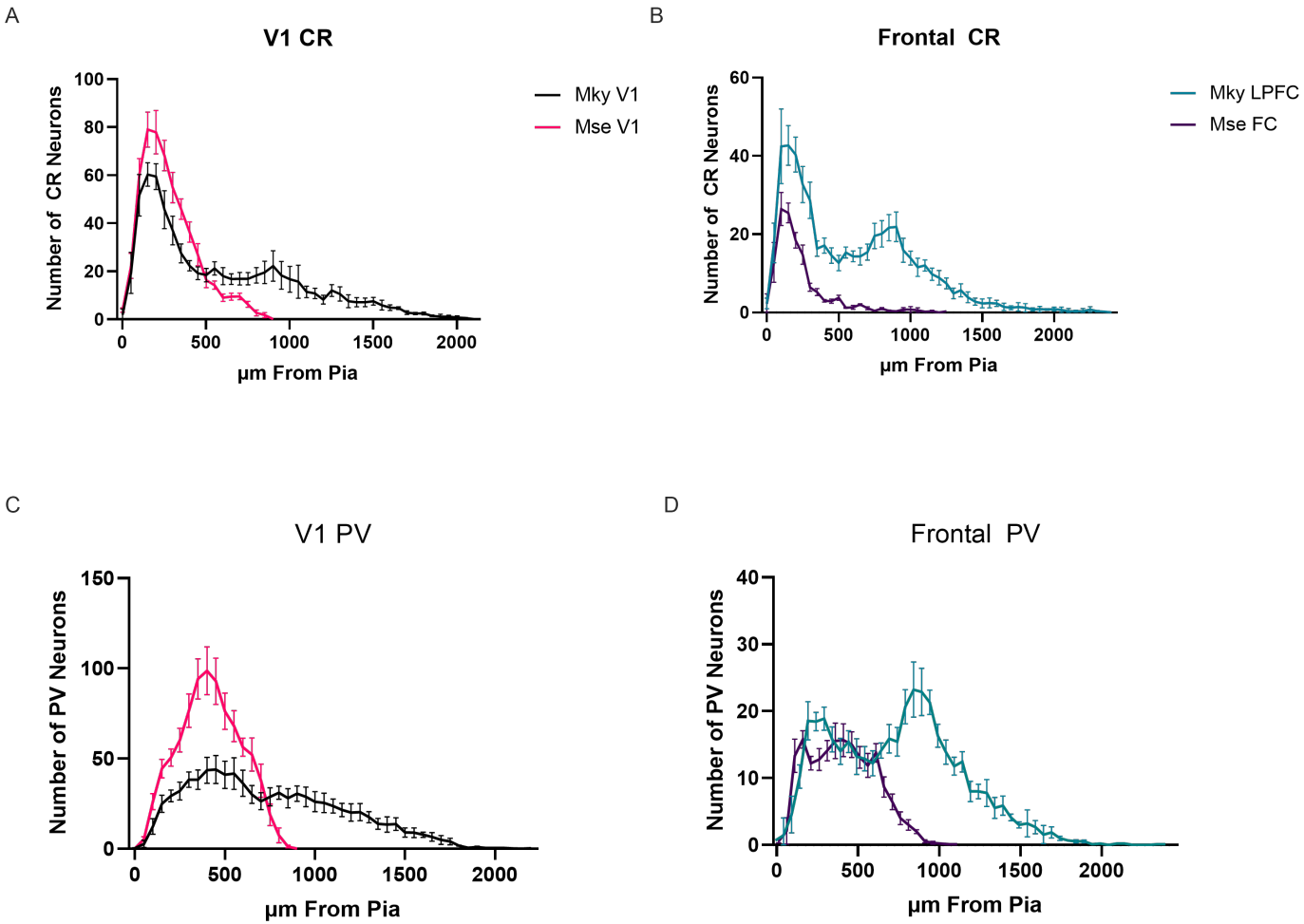

Figure 12: Comparison of the distribution of CR and PV neurons between species A) compares CR in monkey and mouse V1. B) Compares CR in monkey LPFC and mouse FC. C) compares PV in monkey and mouse V1. D) compared PV in monkey LPFC and mouse FC. The bins are 50µm.

Table 3: Inter-areal and Inter-species significances for CR neuronal distances.
Table 3 shows the results of T-tests for every 50µm bin. P<.05 = *, P<0.01 = **, P<0.001 = ***, P<.0001 = ****

	Mky V1	**Mse FC**
Mky LPFC	50–150*	100–150* 150–200*** 200–250**** 250–350*** 350–450**** 450–550*** 550–650**** 650–700*** 700–800**** 800–1100***
Mse V1	100–200* 200–350** 350–400*** 400–500** 500–650* 800–900*	100–150*** 150–200**** 200–250*** 250–450**** 450–500*** 500–550** 550–600**** 600–650** 650–750*** 750–800**

Table 4: Inter-areal and Inter-species significances for PV neuronal distances.
Table 4 shows the results of T-tests for every 50µm bin. P<.05 = *, P<0.01 = **, P<0.001 = ***, P<0.0001 = ****.

	Mky V1	**Mse FC**
Mky LPFC	150–350* 350–650** 650–700* 750–800* 1100–1400*	200–250* 250–300** 300–350* 650–700* 700–800** 800–850*** 850–900**
Mse V1	150–200* 250–300* 250–400** 400–450* 550–750* 750–900**	100–150* 150–200*** 200–300**** 300–350*** 350–400**** 400–600*** 600–650**** 650–750** 750–800*

Normalized distances of CR and PV neurons

Since brain regions have differences in cortical depths across species, the soma-to-pia distance for each counted neuron was normalized to the total cortical depth for each animal to assess inter-areal and inter-species differences in neuronal distribution patterns. Fig. 13A is an image of monkey LPFC with the contours used to delineate the soma locations and pia superimposed. Percent distance from pia for each neuron was determined by taking distance from pia and dividing it by the sum of the distances to pia and white matter. Normalizing the distances makes it possible to make inter-areal and inter-species layer comparisons.

Figure 13B shows the ratio of CR to PV neurons as a function of percent distance from pia. The y-axis shows the $\log_{10}$ of the CR:PV ratio. All of the groups have more CR neurons compared to PV neurons above 10% distance from pia. Monkey V1 and LPFC follow similar patterns across the depth of the tissue, the major difference is that MonkeyLPFC has proportionally more CR neurons from 20% distance from pia through the rest of the tissue. Mouse V1 has the smallest CR:PV ratio of the 4 groups after 55% distance from pia. Mouse FC has more PV than CR neurons from 10% to 60% distance from pia.

Figure 13C shows the CR neurons distribution as a percent distance from pia. All of the 4 brain areas have a peak of concentration of CR neurons from 0–20% of total cortical depths, falling within layer 2 to upper layer 3. Monkey LPFC has significantly more CR neurons than Mouse FC from 15–65% and 80–100% distances from pia ($P<0.05$). Monkey V1 has significantly more CR neurons compared to mouse V1 between 5–20%

distance from pia ($P<0.05$). Monkey V1 has significantly more CR neurons from 30–40 and 55–60% distances from pia compared to monkey LPFC ($P<0.01$). The differences between monkey V1 and mouse FC are more pronounced than the differences between monkey V1 and monkey LPFC. There are significantly more CR neurons in mouse V1 than FC from 5–60% ($P<0.01$), 70–75% ($P<0.05$) and 80–95% ($P<0.05$) distances from pia, and they are dispersed over a wider distance compared to monkey inter-areal differences. Mouse V1 has a sharper peak in Fig. 11D and Fig. 12A, but the peak is spread out when the distances are normalized. The peak for mouse V1 is located deeper than the other brain areas. Monkey LPFC had significant more CR neurons compared to mouse FC from 15–65% ($P<0.05$), 70–75% ($P<0.01$), and 80–100% ($P<0.01$) distances from pia. A noteworthy feature of Mouse FC is that it is non-significant from both mouse V1 and Monkey LPFC 65–70% and 65–80% distance from pia.

PV neuron distribution was compared between the 4 groups (Fig. 13D). PV neurons have more inter-species and inter-areal differences than CR neurons. Compared to mouse V1, monkey V1 has significantly more PV neurons 10–15% ($P<0.01$) and 20–35% ($P<0.01$) distances from pia. Conversely, mouse V1 has significantly more PV neurons from 50–60% distance from pia compared to monkey V1($P<0.05$). The peak for mouse V1 is located further from the pia compared to the peak in monkey V1. Monkey V1 has significantly more PV neurons than monkey LPFC does from 20–55% distance form pia ($P<0.05$). This difference occurs at the peak of PV neurons in monkey V1. Mouse V1 has significantly more PV neurons from 30–90% distance from pia compared to mouse FC ($P<0.01$). Monkey LPFC has significantly more PV neurons compared to mouse FC at the

60–65% ($P<0.05$) and 75–80% ($P<0.05$) distances from pia. This is the same region in Monkey LPFC that increase in PV neurons relative to the rest of the tissue.

The relative frequency graphs (Figs. 13E, F) make it easier to visualize comparisons between mouse FC and the other groups. Tests of significance could not be conducted because the relative frequency is the aggregation of all of the neurons from all of the animals per each bin relative to the total number of neurons for a given group. Fig. 13E shows the relative frequency of CR neuronal distribution. It is more obvious that there is a relatively high concentration of CR neurons in the first 30% of mouse FC. Mouse V1 and FC have one obvious peak compared to monkey V1 and LPFC which have one large peak at 20% followed by a smaller peak at 60% and 75% for monkey LPFC and V1 respectively.

Monkey LPFC and mouse FC have less PV neurons than the monkey V1 and mouse V1 (Fig. 13F). Inter-areal differences are more distinct for the number of PV neurons compared to CR neurons as seen in Fig. 13C, D. Due to the lower number of PV neurons in mouse V1 and FC, the relative frequency of PV neurons makes comparison of the trends of the mouse groups compared to the monkey groups more straightforward. Monkey LPFC and mouse FC both have a peak at 20% distance from the pia. However, monkey LPFC has its largest peak at 65%. mouse FC, similar to mouse V1, has one large peak, and monkey V1 also has one main peak. Monkey LPFC is different from the other groups in that it has 2 peaks for the distribution of PV neurons.

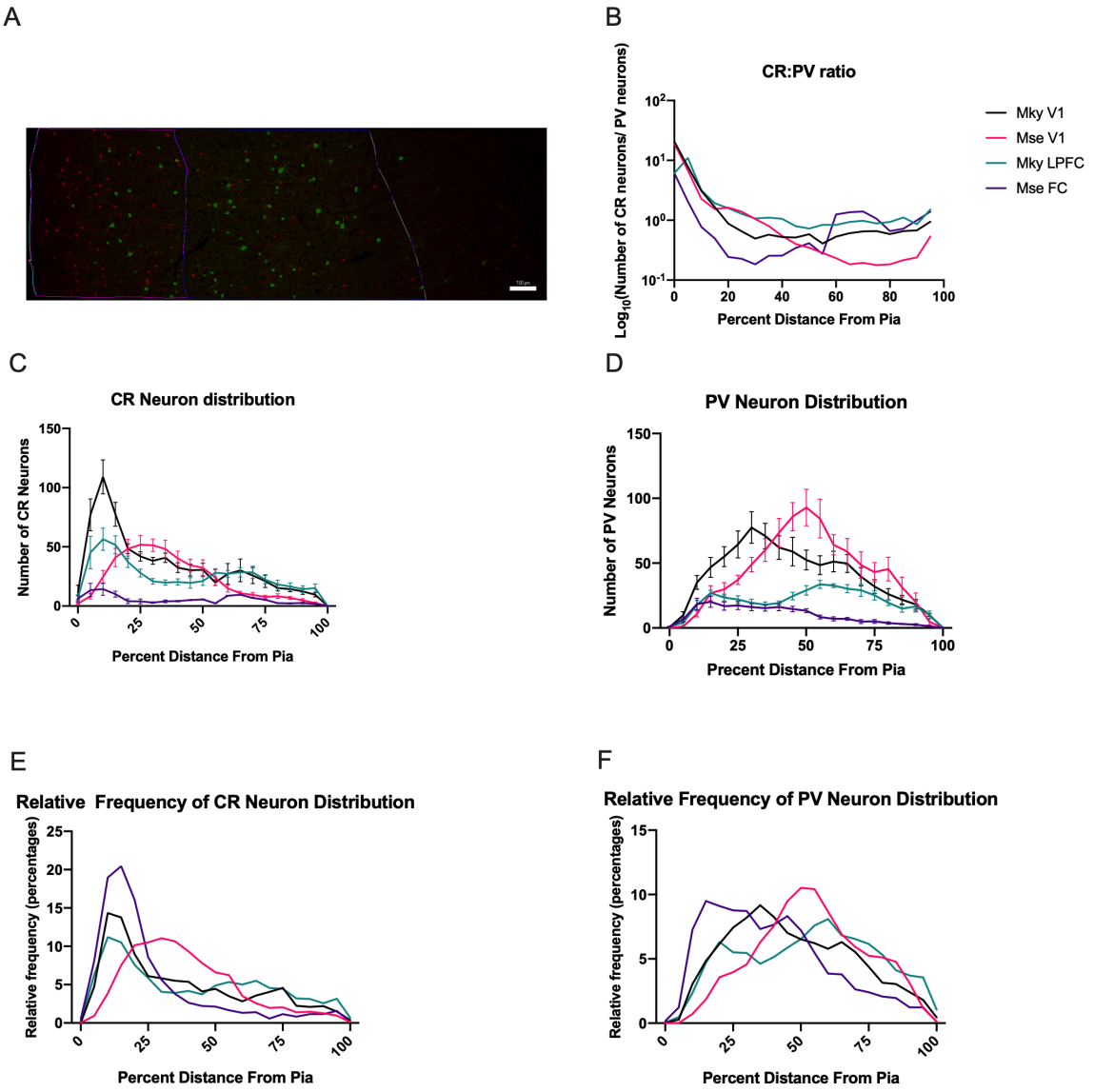

Figure 13: CR and PV neuronal percent distance from pia A) Monkey V1 immunostained tissue with contours marked. Pia (light blue), white matter (yellow), Layers 1–3 (pink), layers 4–6 (dark blue). B) Ratio of CR:PV as a function of percent distance from pia. C–D) CR and PV neuronal distribution. The bins are 5%. The % distance from pia is calculated using the distance of each neuron from the pia contour and the white matter contour. E–F) Relative frequency of CR and PV neuronal distribution. The relative frequency is calculated using the number of neurons per bin compared to the total neurons. The bin size is 5%.

Table 5: Inter-areal and Inter-species significances for CR neuronal distances from pia. ANOVAs were conducted for each bin. Bonferroni post-hoc analysis were performed on all of the 5% bins. P<.05 = *, P<0.01 = **, P<0.001 = ***, P<0.0001 = ****.

	Mky V1	**Mse FC**
Mky LPFC	30–40*** 55–60**	15–20* 20–25**** 25–30*** 30–35**** 35–45*** 45–55** 55–60**** 60–65* 70–75** 80–85*** 85–90**** 90–100**
Mse V1	5–10*** 10–15**** 15–20* 30–35***	5–10** 10–15**** 15–20*** 20–50**** 50–60*** 70–75* 80–90** 90–95*

Table 6: Inter-areal and Inter-species significances for PV neuronal distances from pia. ANOVAs were conducted for each bin. Bonferroni post-hoc analysis were performed on all of the 5% bins. P<.05 = *, P<0.01 = **, P<0.001 = ***, P<0.0001 = ****.

	Mky V1	**Mse FC**
Mky LPFC	0–5** 20–25** 25–30*** 30–45**** 45–50** 50–55* 65–70*	60–65* 75–80*
Mse V1	10–15** 20–25** 25–35* 50–55** 55–60*	30–35** 35–70**** 70–75*** 75–85**** 85–90***

Laminar distribution of PV and CR neurons

The relevance of cortical depth is based on the presence of distinct layers that receive distinct inputs and outputs. The cytoarchitecture of cortical layers differ between areas and species. We thus binned the cortical depths of each cell counted into discrete laminar groups- Layers 1, 2–3, 4, and 5, 6 -identified using cytoarchitecture and published layer dimensions by other investigators (Pierri et al. 1999, Xu et al., 2016, Anastasiades et al., 2018). These areal limits can be found in Table 1. Layer 4 is not prominent in Mouse FC, which is reflected in the bin size and the amount of neurons observed in our experiments. For Figures 14 A–D, 2-way repeated measures ANOVAs were conducted for each graph with the dependent variables of species with 2 levels, V1 and frontal cortices, and layer. All of the within subject factors were significant as follows: Region, region*species, layer, region*layer ($P<0.001$), layer*species, region*layer*species ($P<0.01$). Bonferroni post-hoc tests were conducted for every layer as well. Mouse FC has significantly fewer CR neurons compared to mouse V1 and monkey LPFC in Layers 2–5 ($P<0.01$). Majority of CR neurons are located in L2/3 for all of the groups (Fig. 14A). CR laminar distribution is relatively similar between monkey V1, mouse V1, and monkey LPFC. Monkey V1 and LPFC CR are only significantly different in Layers 2/3 and Layer 6 ($P<0.05$).

Fig. 14B shows the distribution PV neurons binned by laminar groups. Notably, there were no significant interactions between region*species. Interactions of region, layer, region*layer, region*layer*species were all significant ($P<0.001$). Layers 2/3 only has significant inter-areal differences ($P<0.0001$). Layer 4 exhibits significant inter-areal

differences within monkey ($P<0.001$) and mouse ($P<0.0001$) as well as significant differences between mouse V1 and FC ($P<0.05$). Mouse V1 has significantly more PV neurons in Layer 5 compared to monkey V1 ($P<0.001$) and mouse FC ($P<0.0001$). In Layer 5, Mouse V1 is the most distinct of the species and brain regions in terms of the laminar distribution of PV neurons. Finally, there are significantly more PV neurons in Layer 6 of mouse V1 compared to the monkey V1 ($P<0.01$) and mouse FC ($P<0.001$), but there are fewer PV neurons in Layer 6 (144.7 ± 30.8) compared to L5 (348.8 ± 46.1).

As we found differences in the number of PV and CR neurons in each layer, we next investigated whether the proportion of CR and PV neurons in each layer differed between areas and species. Thus, we expressed the number of neurons in each layer as a % of the total number of CR or PV neurons within the entire section. This presentation of laminar distribution shows that mouse FC has a distinct proportion of CR and PV neurons in each layer compared to the other groups (Fig. 14C). All of the interactions were significant: region, region*species ($P<0.05$), layer, layer*species, layer*region*species ($P<0.001$). A 2-way Bonferroni post-hoc tests were conducted for every layer. There is a significantly higher proportion of CR neurons in Layer 1 mouse compared to monkey LPFC ($P<0.0001$). Mouse FC also has significantly greater proportion of CR neurons in L2/3 compared to these layers in monkey LPFC ($P<0.0001$) and mouse V1 ($P<0.001$). These findings are in contrast to Mouse FC having a significantly lower proportion of CR neurons compared to monkey LPFC ($P<0.001$) (Fig. 14A). There are no significant differences in the proportion of neurons in L2/3, while that was the layer with the most significances in CR neuronal count differences (Fig. 14A). In addition, there are

significantly lower proportions of CR neurons in L4 of mouse FC compared to monkey LPFC and mouse V1 ($P<0.0001$). Mouse FC has a significantly lower percentage of total CR neurons in L5 compared to monkey LPFC ($P<0.01$) and mouse V1 ($P<0.05$). Mouse FC has significant inter-species and inter-areal differences in L1 and L4, but there were no other significant differences.

Figure 14D shows the normalized number of PV neurons within each bin. The significant interactions were layer, layer*species, and region*layer ($P<0.001$). In L1, there were significantly higher relative frequency of PV neurons in mouse FC compared to the monkey LPFC ($P<0.05$) and mouse V1 ($P<0.05$). There were no significant differences in proportion of PV neurons in L2/3, unlike the significant inter-areal differences in PV neuronal count ($P<0.0001$) (Fig. 6B). There is a significantly lower proportion of PV neurons in L4 of Mouse FC compared to Monkey LPFC ($P<0.001$) and mouse V1 ($P<0.0001$). In L5, there is a significantly greater proportion of PV neurons in mouse V1 compared to monkey V1 ($0<0.05$). This is the only layer where there are differences between monkey and mouse V1. Importantly, when the number of PV neurons was normalized between monkey V1 and LPFC no significant differences were found.

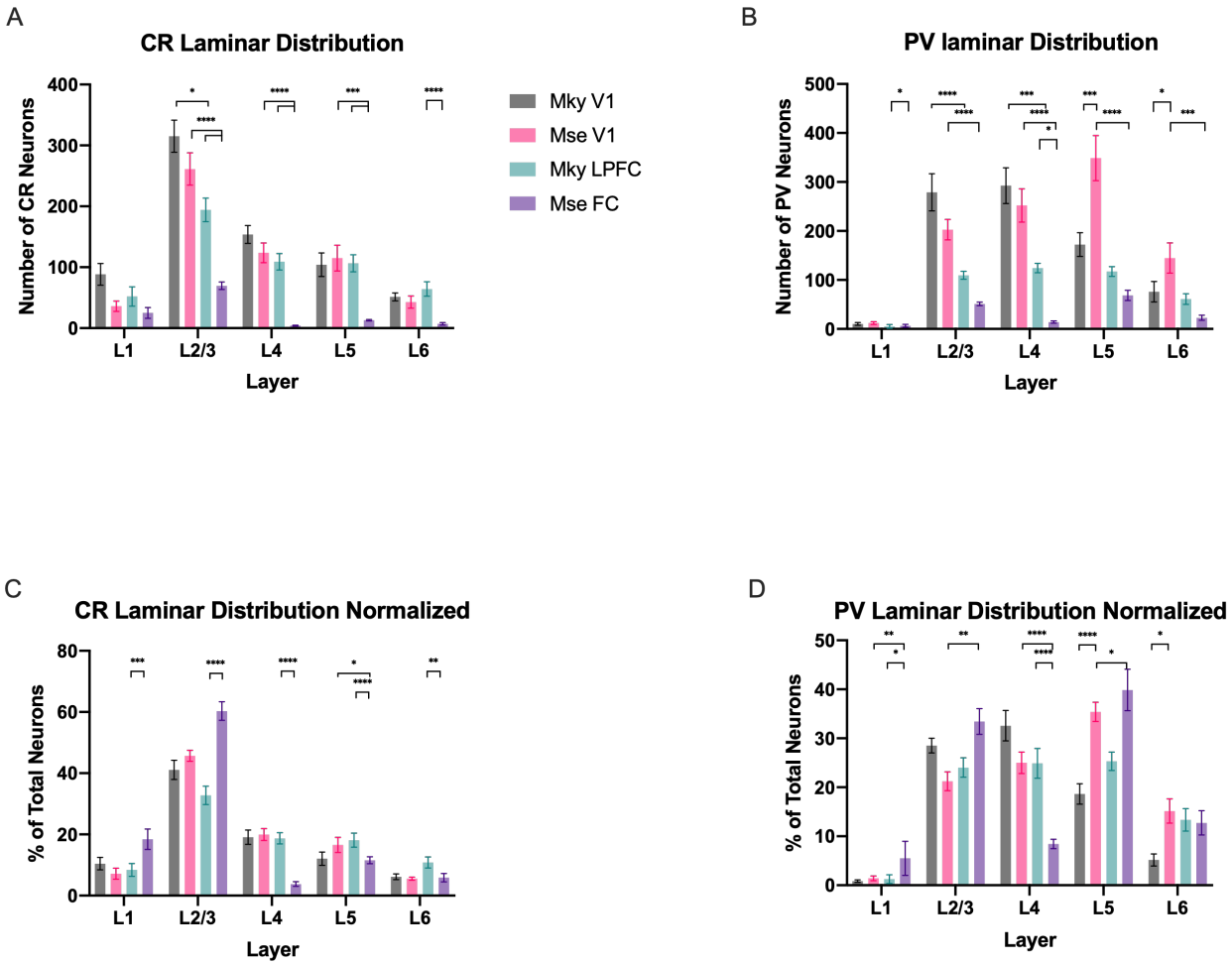

Figure 14: Comparison of the laminar distribution of PV and CR neurons. Table 1 contains the values used to define the bins. Significances were determined using a 1-way ANOVA with Bonferroni post hoc test for each layer. A, B show the number of neurons within each layer. C, D show the bins normalized by taking the number of neurons within each bin and dividing it by the total number of neurons.

Densities of CR and PV neurons

Figure 15 shows the density of CR and PV neurons in upper middle (L1–3) and deep (L4–6) layers. Figures 10B and 11A show how the boundaries for the upper and lower layers were defined. Figure 15A shows the only significant differences of CR neuron density in the upper middle layers is between species. This difference is most pronounced between monkey LPFC and mouse FC. There is a significantly higher density of CR neurons in monkey V1 compared to mouse V1 ($P<0.05$). There is also significantly higher density of CR neurons in monkey LPFC compared to mouse FC ($P<0.01$). There is also a significantly higher density of CR neurons in the deeper layers of monkey LPFC compared to mouse FC ($P<0.0001$). This difference is more significant than the differences for monkey LPFC and mouse FC in the upper middle layers. Monkey V1 is has significantly higher density than mouse V1 ($P<0.05$) and lower density than monkey LPFC ($P<0.05$). The inter-species differences are greater in the frontal regions, and only the frontal regions have significant inter-species differences in the lower layers.

Only the upper middle layers have inter-species and inter-areal differences in PV density (Fig. 15B). Monkey V1 has a significantly higher density of PV neurons compared to mouse V1 ($P<0.01$). The inter-species differences are more notable than the inter-areal differences. There are no significant relationships in the deeper layers. Monkey V1 is the most distinct group for PV neurons, whereas monkey LPFC is the most distinct group for CR neurons.

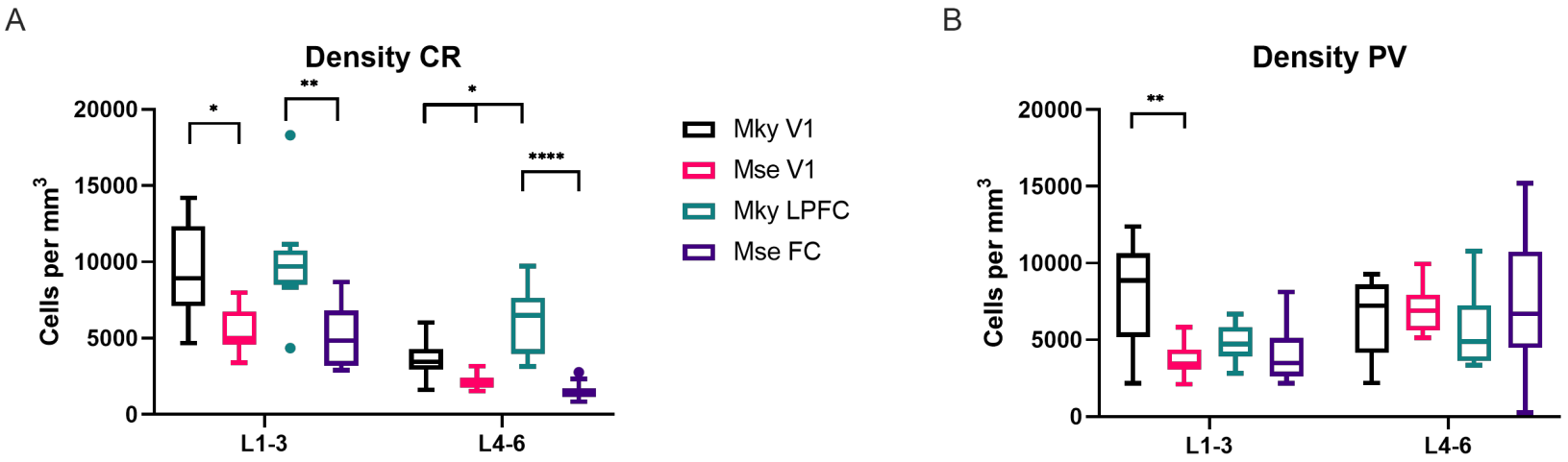

Figure 15 Densities of CR and PV neurons in L1–3 and L4–6. Significances were determined by performing a two-way ANOVA and the Bonferroni post-hoc analysis

Particle Analysis and Colocalization

VGAT particle analysis was conducted across the entire 40x image for a given section, but the images that were analyzed only represent L1–3 because those were the layers that the neurons resided in for the reconstructions. Figure 16A shows the VGAT channel within a zoomed in region of monkey V1. Vgat particles are dispersed and encompass much of the image. There are visible punta some of which form rings- apparently around the somata of pyramidal neurons, indicative of perisomatic inhibition. Qualitatively there appear to be more diffuse VGAT puncta in mouse V1 (Fig. 16B) compared to monkey V1 (Fig. 16A). Monkey LPFC (Fig. 16C) has higher density of VGAT puncta than mouse FC (Fig. 16D). The particle analysis indicates significant inter-species differences in inhibitory synapses (Fig. 16F). There is a significantly higher density of Vgat particles in monkey V1 compared to mouse V1 ($P<0.0001$) and monkey LPFC compared to mouse FC ($P<0.001$).

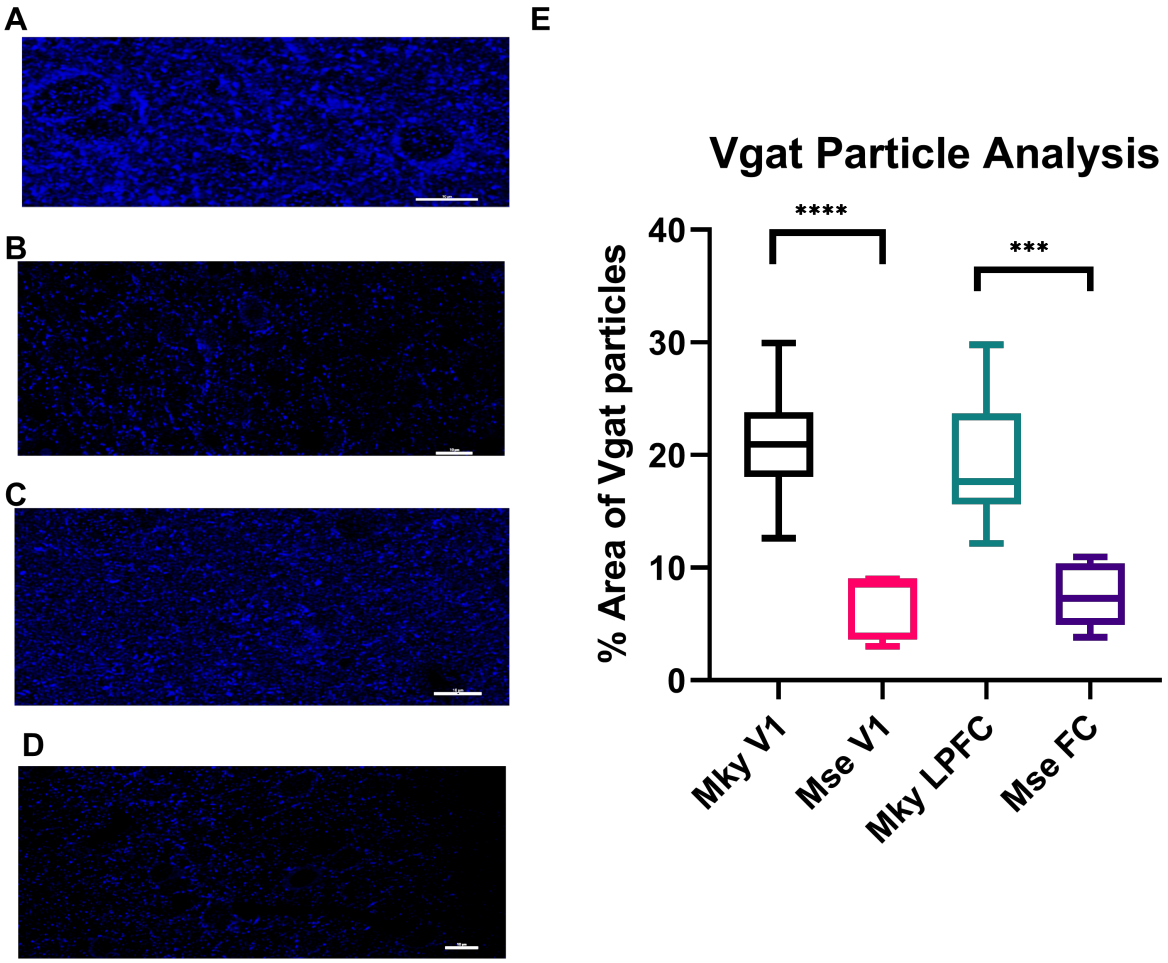

Figure 16 Particle Analysis of VGAT: A–D) show a zoomed in image of a 40x image showing the VGAT channel (blue). A) 40x scan of monkey V1. B) 40x scan of mouse V1. C) 40x scan of monkey LPFC. D) 40x scan of mouse FC E) The Vgat Particle Analysis shows the % area of the scanned that contained VGAT particles. One-way ANOVAs and bonferonni post hoc analysis were conducted for Fig. 16E. Scale bars 10μm.

The density of CR and PV neurons and percent area occupied by VGAT particles were plotted for each section. Linear regressions for CR neuronal density x percent area occupied by VGAT particles and PV neuronal density x percent area occupied by VGAT particles are shown in Fig. 17a, b. Both the density of CR and PV neurons are weakly correlated with the percent area occupied by VGAT particles. Percent area of VGAT particles is more positively correlated with density of CR neurons ($R^2 = 0.31$) compared to PV neurons ($R^2 = 0.17$). This suggests a relationship between synaptic and population properties of INs.

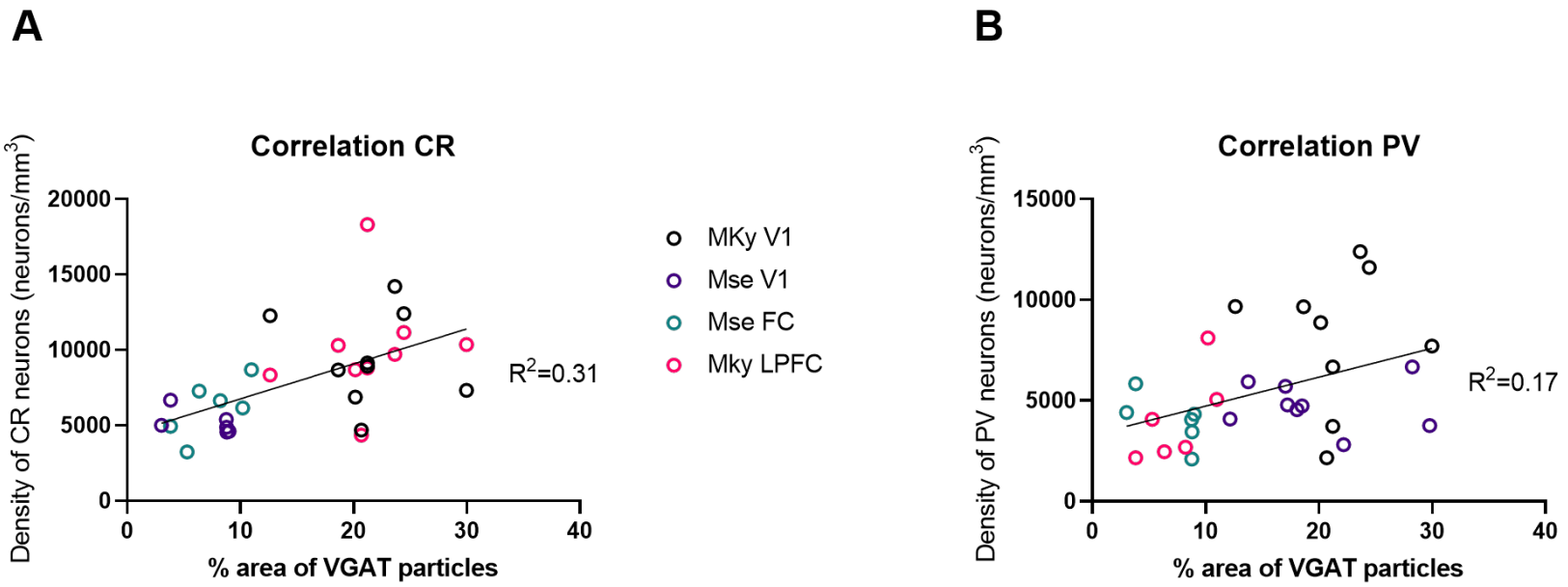

Figure 17: Correlation of density of CR and PV neurons with VGAT particle analysis. A) Linear correlation between % area of VGAT particles and Density of CR neurons. B) Linear correlation between % area of VGAT particles

CR colocalization analysis was conducted across the entire 40x image for a given section, the images only represent Layer 1–3 because those were the layers that were included in the 40x images. In Monkey V1, Two of the CR neurons have Vgat particles colocalized around the soma, indicating perisomatic inhibition onto CR (Fig. 18A). The CR neuron on the left side of the panel is projecting a dendrite around the soma of a PV neuron seen in (Fig.19A). This projection also has colocalized Vgat particles. Mouse V1 has more diffuse VGAT particles and more CR background (Fig. 18B). Monkey LPFC (Fig. 18C) has more robust VGAT density and a distinct dendrite connecting to the soma on the top of the image. compared to Mouse FC (Fig. 18D). CR colocalization has less pronounced inter-species differences compared to particle analysis. There is a significantly more Vgat+/CR+ colocalization in monkey LPFC compared to mouse FC ($P<0.01$)

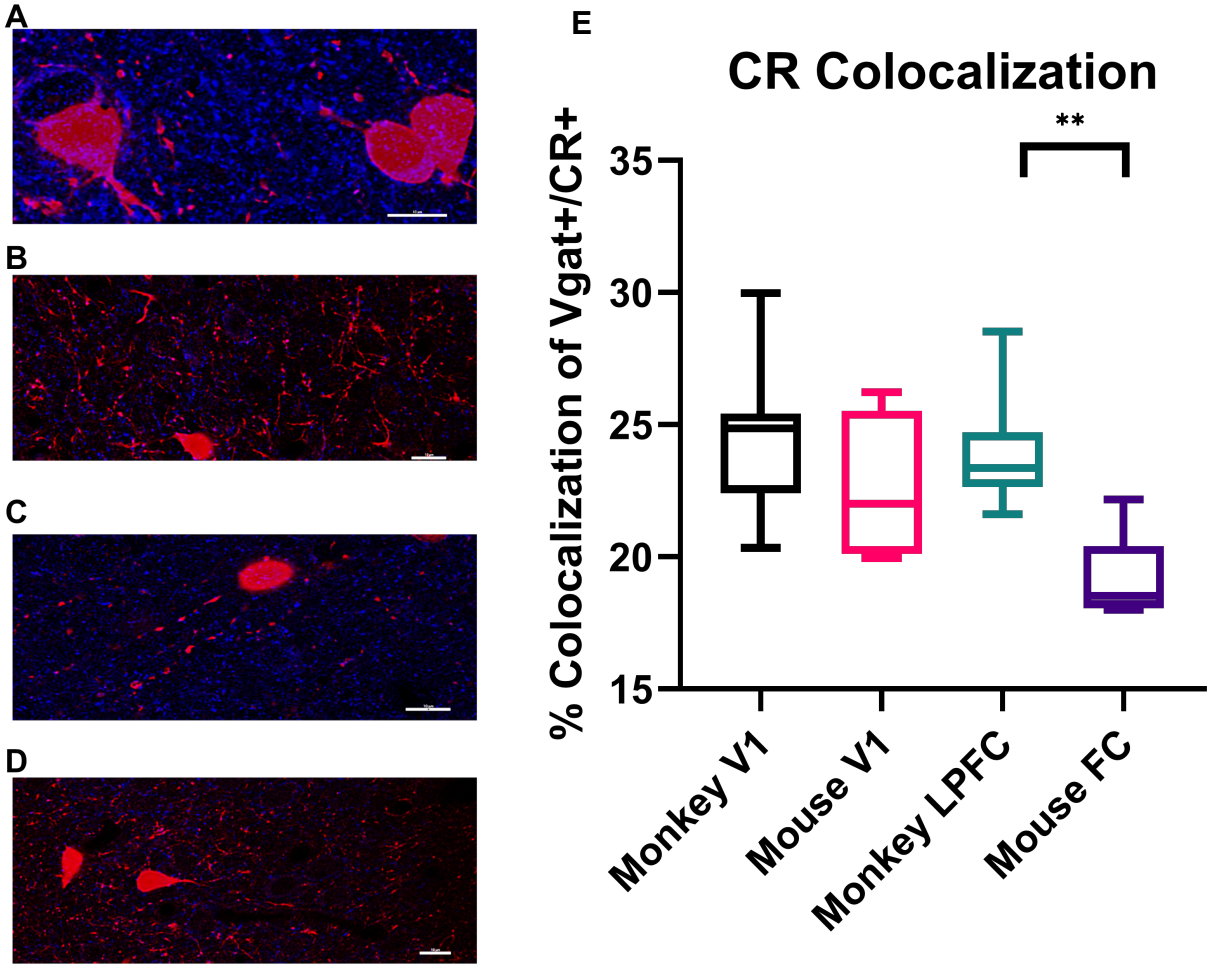

Figure 18 Colocalization of VGAT+/CR+: A–D) show a zoomed in image of a 40x image showing the VGAT (blue) and CR (red) channels. A) 40x scan of monkey V1. B) 40x scan of mouse V1. C) 40x scan of monkey LPFC. D) 40x scan of mouse FC E) The CR Colocalization shows the Manders Correlation Coefficient of VGAT+/CR+. One-way ANOVAs and bonferonni post hoc analysis were conducted for Fig. 18E. Scale bars 10µm.

PV colocalization analyses was conducted across the entire 40x image for a given section. In monkey V1, there are Vgat puncta surrounding the soma of the PV neuron on the left side of the panel (Fig. 19A). Mouse V1 has more diffuse VGAT particles and more PV background (Fig. 10B). Monkey LPFC (Fig. 19C) has more robust VGAT density and distinct dendrites compared to Mouse FC (Fig. 19D). The PV soma also has perisomatic inhibition from an adjacent CR neuron (Fig. 18A). There is a significantly more Vgat+/PV+ colocalization in mouse V1 compared to monkey V1 ($P<0.01$). Colocalization only has significant inter-species; however, it is only significant in V1 for CR and frontal cortices for PV.

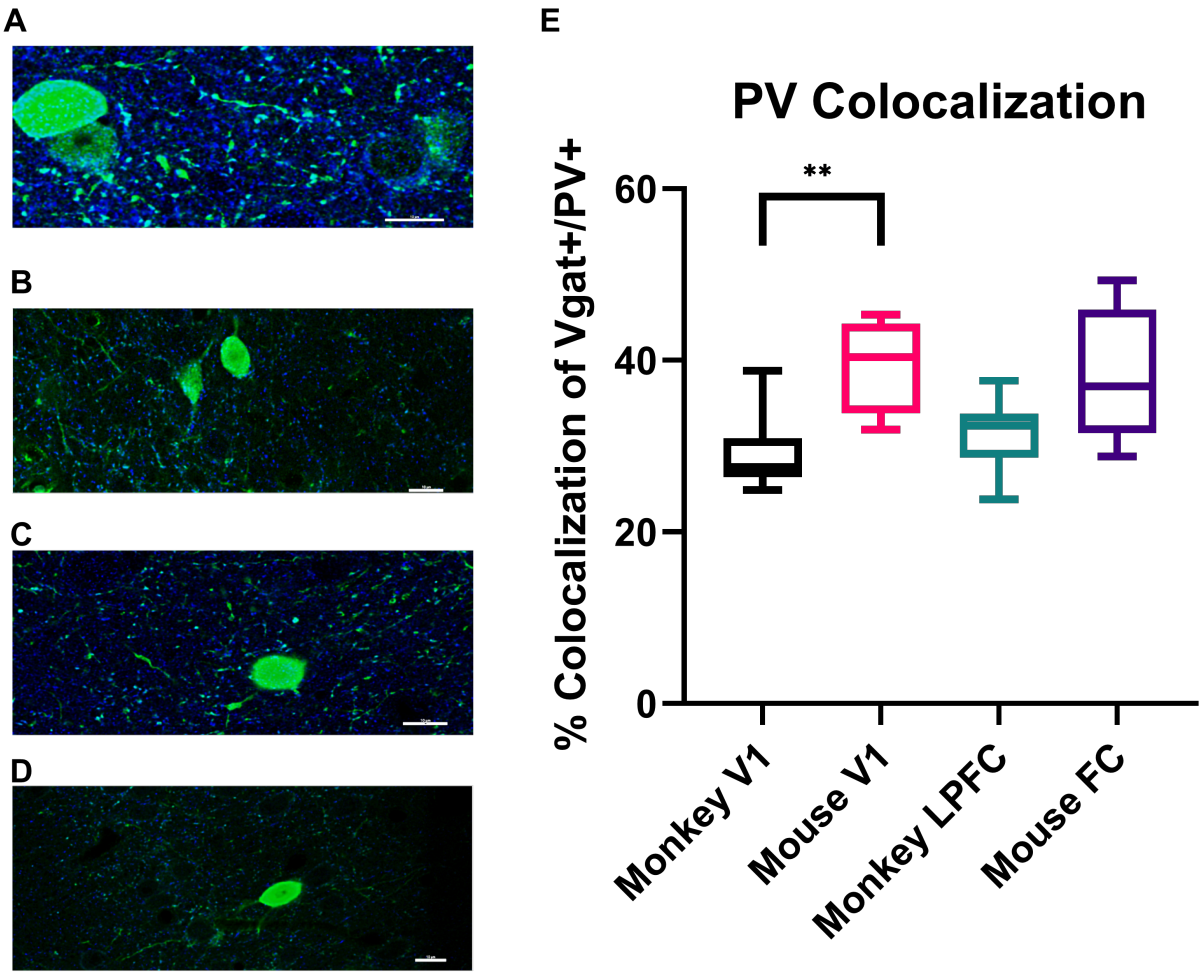

Figure 19 Colocalization of VGAT+/PV+ A–D) show a zoomed in image of a 40x image showing the VGAT (blue) and PV (green) channels. A) 40x scan of monkey V1. B) 40x scan of mouse V1. C) 40x scan of monkey LPFC. D) 40x scan of mouse FC E) The PV Colocalization shows the Manders Correlation Coefficient of VGAT+/PV+. One-way ANOVAs and Bonferroni post hoc analysis were conducted for Fig. 19E. Scale bars 10μm.

Discriminant Analysis and Algorithmic HierarchicalCluster Analysis

Group clustering was determined using discriminant analysis (DA). The analysis includes data from Louis Park's CR morphologies. DA revealed how groups segregated and what factors contributed the most to group differences. Nine variables were assessed which includes: CR and PV density in upper and lower layers, Vgat particle analysis, dendritic nodes, cell body surface area, cell body volume, mean dendritic length and soma to pia distance. The analysis was run seperately for density, morphology, and all variables together. Figure 9A–C shows the DA for the density variables. The monkey groups are segregated from the mouse groups across the aggregated X variables axis, whereas monkey V1 differs from the mouse groups and monkey LPFC along the aggregated Y variable axis. The canonical correlation, *r*: discriminant function $df_1 = 0.908$, $df_2 = 0.701$, $df_3 = 0.042$; Wilks' λ: 1–3 = 0.66, 2–3 = 0.881, 3= 0.991, ($P < 0.0001$) (Fig. 20B, C). The density of PV neurons in the upper layers are assigned the greatest contribution to seperation along the Y axis, making the density of PV neurons in the upper layers the variable which primarily seperates monkey V1 from the other groups. Most of the inter-species difference occurs along the x axis, which is influenced primarily by CR density in the upper and lower layers. There is far less group segregation in terms of CR neuronal morphology. The $df_1 = 0.494$, $df_2 = 0.333$, $df_3 = 0.093$; Wilks' λ: 1–3 = 0.594, 2–3 = 0.851, 3= 0.958, ($P < 0.001$) (Fig. 20D–F). The most distinct group is mouse V1 which is discriminanted primarily based on the number dendritic branch points. The combination of all of the variables yields more inter-species segregation, primarily due to the addition of the Vgat particle analysis variable; $df_1 = 0.948$, $df_2 = 0.845$, $df_3 = 0.449$; Wilks' λ: 1–3 = .011, 2–3 = 0.150, 3= 0.641,

$P < 0.0001$ (Fig. G–I). Figure 20C shows that inter-species differences are the biggest contributing factor to differences in Particle Analysis and Colocalization of Vgat. The inter-areal differences are more pronounced in mouse compared to monkey.

Algorithmic hierarchical clustering (AHC) was performed using the same 9 variables used in the DA. The dendrogram plot (Fig. 21D) is based on squared Euclidean distances. The AHC shows that the groups are first clustered by species then brain area (r: $df_1 = 1$, $df_2 = 0.97$). There are fewer differences between mouse FC and V1 ($d^2 = 749$) compared to those between Monkey LPFC and V1 ($d^2 = 4115$).

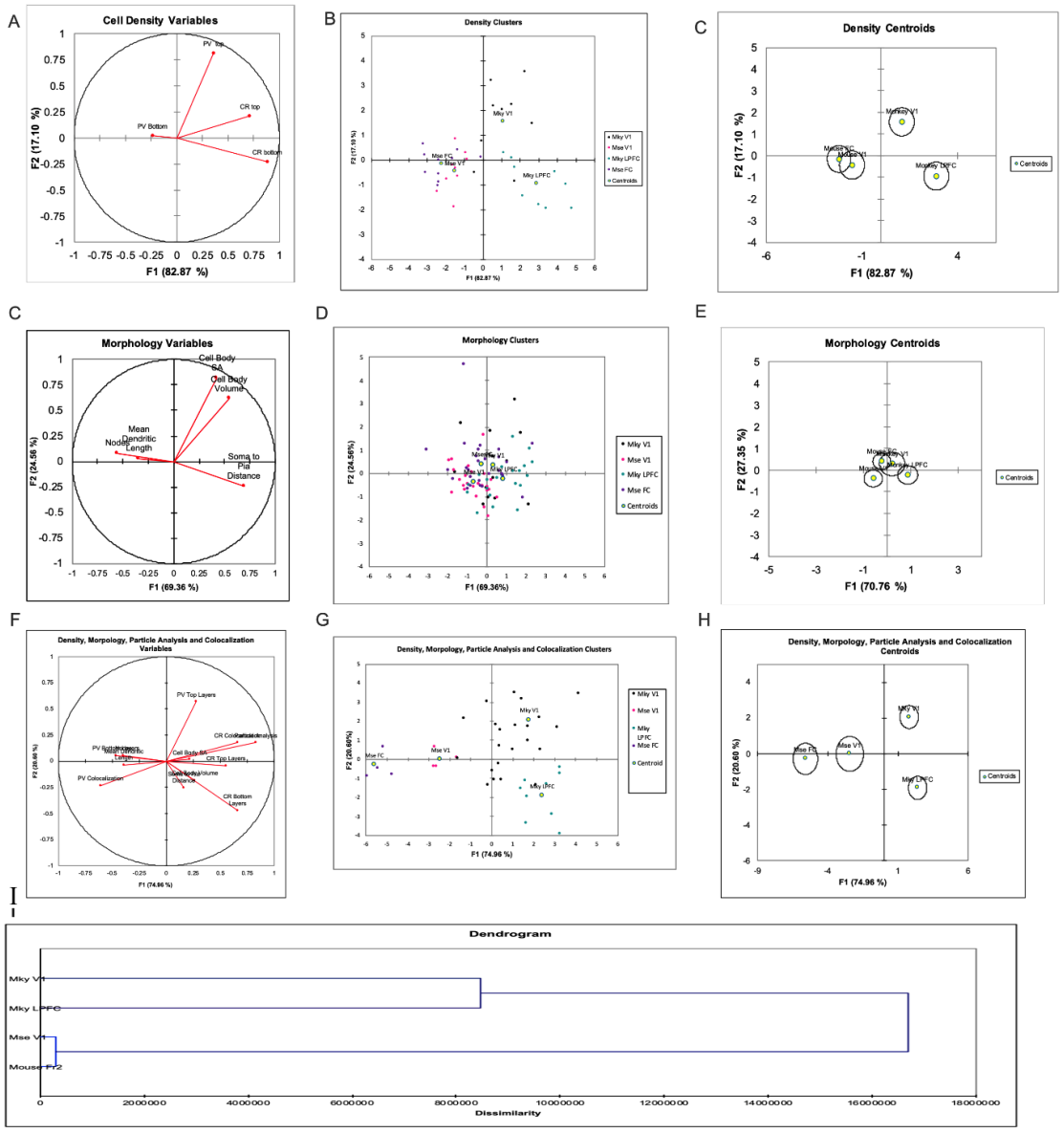

Figure 20: Discriminant analyses for all 4 brain regions A–C) DA for the neuronal densities. Weight of variables in determining the clustering (left). The neuronal density cluster plot (middle). The neuronal density centroid plot shows only the centroids (right). D–F) Discriminant analysis for CR Morphology for all 4 tissue groups. Weight of the variables in determining the clustering of the 4 groups of tissue (left). The CR morphology cluster plot (middle). The CR morphology centroid plot shows only the centroids (right). G–I) Discriminant analysis for the CR Morphology, CR and PV Density and Vgat Particle Analysis. Weight of variables in determining the clustering (left). The Morphology, Density, and Particle Analysis cluster plot (middle) The centroids are shown by themselves in the plot on the right. I) Hierarchical cluster analysis based on morphology, density, particle analysis, and colocalizations. Hierarchical cluster tree shows the relative (dis)similarities of the 4 groups

DISCUSSION

Interneurons play an integral role in balancing the excitatory signals of pyramidal cells through inhibitory GABAergic signaling. CR and PV neurons are two classes of INs that have different morphologies and distributions. Our data reveals that there are differences in CR and PV distribution between species, brain region and layer. The best way to analyze the distribution is by layer instead of distance from pia because of the functional anatomical differences between layers. The difference in CR and PV distribution were greatest between layers. In fact, for the distribution of PV there was no significant interaction between region and species without the factor of layer.

The somata of CR neurons are found predominantly in layer 2/3. For all 4 of the groups, this was the layer that had the most CR neurons (Fig. 14A, C). This agrees with the work of Gabbot and Colleagues (Gabbot et al., 1997, Gabbot and Bacon 1996a, b). Mouse FC is the most distinct group compared to monkey LPFC, V1 and mouse FC in terms of CR distribution. The only difference that does not include mouse FC is in L2/3, where there are significantly more CR neurons in monkey V1 compared to LPFC (Fig. 14A). However, when evaluating the percentage of CR neurons in L2/3 compared to total neurons, there are no significant differences between monkey V1 and LPFC (Fig. 14C). There are significant differences in the density of CR neurons as a function of volume in the upper middle layers of Monkey V1 and LPFC (Fig. 15A). There are significantly higher density CR neurons in monkey V1 and LPFC compared to mouse FC and V1, but there are no significant differences between monkey V1 and LPFC (Fig. 15A). This could be due to the inclusion of L1 in the analysis. If we are able to effectively utilize the DAPI staining in

future studies we will be able to further segregate the layers for the density analyses. Mouse FC was also the most distinct brain region in terms of distribution of CR neurons. Mouse FC had the smallest volume scanned compared to mouse V1 and monkey LPFC and V1.

Our data complements observations of differences in L2/3 pyramidal cells of monkey and mice frontal and visual cortices. Monkey V1 L2/3 pyramidal neurons have the lowest frequency and amplitude of spontaneous EPSC's and lowest spine density compared to monkey LPFC, mouse V1 and mouse FC. These neurons are highly excitable and they have lower spine density than monkey LPFC, mouse V1 and mouse FC (Gilman et al., 2017). However, there are more asymmetric synapses in both of the mouse regions compared to both of the monkey regions (Hsu et al., 2017). Monkey LFPC has lower density of pyramidal cells compared to monkey V1, which can explain the decrease in average spine density per individual pyramidal cell in monkey V1 compared to monkey LPFC. There are more CR neurons in L2/3, which send inhibitory signals onto pyramidal cells in L2/3. This indicates differences in excitatory and inhibitory signaling occurring between Monkey LPFC and V1, but this inter-areal phenomenon does not occur in mouse FC and V1.

Dendritic morphology is an important determinant of electrical properties of neurons. The morphology data from the accompanying project done by Louis Park indicates that the dendrites of bipolar CR neurons are long and can extend down into L4. Sholl analysis shows that there is an increase in the diameter of CR neurons in mouse V1 150 μm and monkey V1 at 250μm, that would put the dendrites in L4 (Xu et al., 2016). Differences in length, diameter, and branch angle of dendrites cause variability in the cable

properties of neurons (Luebke, 2017). The increase in diameter allows for more sites of synapses, integration of signals, and signal processing. In bipolar CR cells, the distal dendrites receive input from the thalamus, other bipolar cells and long-distance cortical axons. There is a high count of PV neurons in L4, so they could also have inputs onto the dendrites of L2/3 CR neurons.

Differences in excitatory and inhibitory balance can cause changes in neural circuitry. L2/3 pyramidal cells form cortico-cortical connections (Luo et al., 2017). Inhibitory signals play an important role in circuit dynamics and preserving the temporal fidelity of signals. CR neurons have GABAergic signaling with FS-PV neurons that strongly inhibit L2/3 pyramidal cells, this disinhibits pyramidal cells (Cauli et al., 2014). They can also be involved in feedforward inhibition, which is effective for inhibiting neurons in deeper layers of cortex (Saffari et al., 2019). Taken together, CR neurons integrate inputs from a variety of layers and long-distance axons and can inhibit deep downstream pyramidal cells and adjacent FS-PV cells. Inhibiting FS-PV cells causes the disinhibition of L2/3 pyramidal cells which send excitatory cortico-cortical signals.

The significantly greater amount of CR neurons in L2/3 of V1 compared to LPFC suggests further specialization between brain regions that exists in monkeys, but not in mice. This difference might be due to the highly excitable nature of monkey V1 pyramidal cells (Gilman et al., 2017). The higher amounts of inhibition here may be necessary to prevent over excitation. Disinhibition can also allow the recruitment of task-relevant neurons in response to context specific inputs. This occurs when mice associate visual stimulus with important contexts such as punishment (Hattori et al., 2017).

Most of the somata of PV neurons are found in L2–5. There were more PV neurons in V1 in both species compared to frontal cortices. Notably there were no significant interactions between region*species, significant interactions are layer-dependent. Mouse FC has fewest PV neurons compared to mouse V1 and monkey LPFC and V1 (Fig. 14 B, D). Monkey V1 has significant more neurons in L2/3 compared to LPFC (Fig. 14A). In the upper middle layers, Monkey V1 has significantly higher density of PV cells compared to monkey LPFC and mouse V1 and FC. Mouse V1 has significantly more neurons than monkey V1 in L5. This effect is conserved for the % of PV neurons in L5 of the total PV neurons counted per section. However, the densities in the deep layers are not significantly different. One explanation for this apparently discrepant finding is the inclusion of L6. L6 is a large layer, comprising 25% of the total volume of mouse V1 (Xu et al., 2016).

There are significantly more PV and CR neurons in L2/3 of monkey V1 compared to LPFC. The decrease in spine density in the pyramidal cells of monkey V1 compared to monkey LPFC and mouse FC and V1 is indicative of greater inhibition in monkey V1. We were unable to reconstruct PV neurons due to high background, but the morphology of PV cells has been characterized in other studies. PV neurons have wide axonal arbor that tends to stay confined to 1 layer (Klausberg et al., 2003). Their wide dendritic arbor and gap junctions with neighbors allows for electrical coupling and synchronous firing (Kawaguchi et al., 2019). PV neurons play an important role in inhibition of L2/3 of pyramidal neurons. PV cells can generate high-frequency gamma oscillations through rhythmic inhibitory signaling onto pyramidal cells (Cardin et al., 2009). They are also involved in lateral inhibition because they can exhibit synchronized control over a wide area of pyramidal

cells. Lateral inhibition allows signal discrimination by assigning specific features to specific neurons, and inhibiting adjacent neurons. Suppressing PV neurons in mouse V1 causes impaired selectivity to contrast and orientation (Atallah et al., 2012). This could be why there are more PV neurons in L2/3 of monkey and mouse V1 compared to monkey LPFC and mouse FC (Fig. 14B). The difference in number of PV neurons in L2/3 of monkey V1 compared to mouse V1 was not significant (Fig. 14B). But, there is a significantly higher density of PV neurons in the upper middle layers of monkey V1 compared to mouse V1 and monkey LPFC (Fig. 15B). Monkeys rely on their vision more than mice who tend to rely more on olfaction and touch, which is a possible explanation for the higher density of PV neurons in monkey V1 (Carandini and Churchland, 2013).

One peculiar finding is that L5 mouse V1 has the highest number of PV neurons compared to all of the groups. In the cortico-thalamic-cortical pathway L5 pyramidal cells send projections to the thalamus, to relay cells that project to cortical areas. In mouse V1, L5 pyramidal cells project to the pulvinar nucleus and the lateral posterior nucleus, which send afferent signals to higher visual areas. They can also send afferent signals to motor areas which sends signals that are involved in helping mice perceive their environment (D'Souza and Burkhalter, 2017). There are also slower oscillations that occur in L5. In mice, layers 4 and 5 have 3–6 Hz oscillations that are similar to alpha oscillations, which are active during the waking state (Senzai et al., 2019). The high number of PV neurons in L5 of mouse V1 are likely involved in the dynamics of signals in the cortico-thalamic-cortico pathway. One limitation of the study was that we were unable to characterize the physiological properties of PV neurons. The physiological properties would provide more

information with the role of PV neurons in oscillations. A further study can be conducted that compares physiological properties of PV neurons in monkey V1, LPFC and mouse V1 and FC.

Monkey V1 and LPFC exhibit a significantly higher density of inhibitory synapses, as represented by VGAT, compared to mouse V1 and FC (Fig. 16E). While there are more symmetric (inhibitory) synapses on spines of pyramidal cells from monkey V1 compared to LPFC, there are not many significant differences in symmetric spine density between monkey V1, LPFC and mouse V1 and FC (Hsu et al., 2017). Mouse FC and V1 also have few differences in excitatory synaptic signaling, but there are substantial differences between monkey V1 and LPFC in excitatory synaptic signaling (Hsu et al., 2017). In terms of density of inhibitory synapses, there were significant differences between the monkey and mouse, but not between monkey V1 and LPFC. There are more VGAT+ boutons colocalized with PV+ boutons than with CR+ boutons (Fig. 18E, 19E). PV neurons have more inhibitory synapses in monkey V1, LPFC and mouse V1 and FC, but CR colocalization with VGAT is a significantly higher in monkey LPFC compared to mouse FC. Mouse FC has the lowest % colocalization of VGAT+ boutons to CR+ boutons. This could be explained by the lower density and number of PV neurons in mouse FC, and PV neurons are frequent targets of CR neurons (Fig 14B, D, 15B). There are significantly fewer VGAT+ boutons colocalized with PV+ boutons in monkey V1 compared to mouse V1 (Fig. 19E). The reduced amount of inhibitory colocalized synapses could be compensatory to the decreased density of spines on L2/3 pyramidal neurons in monkey V1 compared to mouse V1 (Gilman et al., 2017). A limitation of our study was that we could not distinguish

between VGAT + boutons that were colocalized with CR+ and PV+ boutons on dendrites, somata and axons. Therefore, we cannot definitively say whether our observations describe inhibitory signaling of PV and CR neurons. A future study that assesses VGAT colocalization by compartments of neurons would resolve this problem.

The discriminant analysis shows that morphology does not influence the separation of groups as much as density of CR and PV neurons, particle analysis of VGAT and colocalization of VGAT+ boutons to CR+ boutons and PV+ boutons. Particle analysis segregated the brain areas by species and upper middle layers of PV density segregated Monkey V1 from LPFC. Mouse FC and V1 are similar to one another; whereas, monkey V1 and LPFC are not as similar to one another (Fig. 20G). The hierarchical cluster analysis confirmed these findings. The groups are first separated by species, then, monkey V1 and LPFC are more dissimilar from one another than mouse V1 and FC. Mouse V1 and FC are very similar compared to monkey V1 and LPFC (Fig. 20I). The discriminant analysis and hierarchical cluster analysis are consistent with findings in pyramidal cells. In terms of L2/3 pyramidal cells, Monkey V1 was the most dissimilar group. Monkey V1 separated by a branching point from monkey LPFC (Gilman et al. 2017). These data show that while it is convenient to classify INs, they are not generalizable due to species, areal and laminar differences.

REFERENCES

Agnati, L. F., Zoli, M., Strömberg, I., & Fuxe, K. (1995). Intercellular communication in the brain: Wiring versus volume transmission. *Neuroscience*, *69*(3), 711–726. https://doi.org/10.1016/0306-4522(95)00308-6

Amatrudo, J. M., Weaver, C. M., Crimins, J. L., Hof, P. R., Rosene, D. L., & Luebke, J. I. (2012). Influence of highly distinctive structural properties on the excitability of pyramidal neurons in monkey visual and prefrontal cortices. *Journal of Neuroscience*, *32*(40), 13644–13660. https://doi.org/10.1523/JNEUROSCI.2581-12.2012

Anastasiades, P. G., Boada, C., & Carter, A. G. (2018). Cell-type specific D1 dopamine receptor modulation of projection neurons and interneurons in the prefrontal cortex. *BioRxiv*, 370536. https://doi.org/10.1101/370536

Atallah, B. V., Bruns, W., Carandini, M., & Scanziani, M. (2012). Parvalbumin-expressing interneurons linearly transform cortical responses to visual stimuli. *Neuron*, *73*(1), 159–170. https://doi.org/10.1016/j.neuron.2011.12.013

Bekkers, J. M. (2011). Pyramidal neurons. *Current Biology*, *21*(24), R975. https://doi.org/10.1016/j.cub.2011.10.037

Buzsaki, G. (1984). Feed-forward inhibition in the hippocampal formation. *Progress in Neurobiology*, *22*(2), 131–153. https://doi.org/10.1016/0301-0082(84)90023-6

Carandini, M., & Churchland, A. K. (2013). Probing perceptual decisions in rodents. *Nature Neuroscience*, *16*(7), 824–831. PubMed. https://doi.org/10.1038/nn.3410

Cardin, J. A., Carlén, M., Meletis, K., Knoblich, U., Zhang, F., Deisseroth, K., Tsai, L.-H., & Moore, C. I. (2009). Driving fast-spiking cells induces gamma rhythm and controls sensory responses. *Nature*, *459*(7247), 663–667. https://doi.org/10.1038/nature08002

Cauli, B., Zhou, X., Tricoire, L., Toussay, X., & Staiger, J. F. (2014). Revisiting enigmatic cortical calretinin-expressing interneurons. *Frontiers in Neuroanatomy*, *8*, 52. https://doi.org/10.3389/fnana.2014.00052

Chalmers, I., & Glasziou, P. (2009). Avoidable waste in the production and reporting of research evidence. *The Lancet*, *374*(9683), 86–89. https://doi.org/10.1016/S0140-6736(09)60329-9

Czeiger, D., & White, E. L. (1997). Comparison of the distribution of parvalbumin-immunoreactive and other synapses onto the somata of callosal projection neurons in mouse visual and somatosensory cortex. *Journal of Comparative Neurology*, *379*(2), 198–210. https://doi.org/10.1002/(SICI)1096-9861(19970310)379:2<198::AID-CNE3>3.0.CO;2-Z

DeFelipe, J., Hendry, S. H., & Jones, E. G. (1989). Visualization of chandelier cell axons by parvalbumin immunoreactivity in monkey cerebral cortex. *Proceedings of the National Academy of Sciences of the United States of America*, *86*(6), 2093–2097. https://doi.org/10.1073/pnas.86.6.2093

Defelipe, J., González-Albo, M. C., & Elston, G. N. (1999). Distribution and patterns of connectivity of interneurons containing calbindin, calretinin, and parvalbumin in

visual areas of the occipital and temporal lobes of the macaque monkey. *Journal of Comparative Neurology, 412*(3), 515–526. https://doi.org/10.1002/(SICI)1096-9861(19990927)412:3%3C515::AID-CNE10%3E3.0.CO;2-1

DeFelipe, Javier. (1997). Types of neurons, synaptic connections and chemical characteristics of cells immunoreactive for calbindin-D28K, parvalbumin and calretinin in the neocortex. *Journal of Chemical Neuroanatomy*, *14*(1), 1–19. https://doi.org/10.1016/S0891-0618(97)10013-8

DeFelipe, Javier, López-Cruz, P. L., Benavides-Piccione, R., Bielza, C., Larrañaga, P., Anderson, S., Burkhalter, A., Cauli, B., Fairén, A., Feldmeyer, D., Fishell, G., Fitzpatrick, D., Freund, T. F., González-Burgos, G., Hestrin, S., Hill, S., Hof, P. R., Huang, J., Jones, E. G., … Ascoli, G. A. (2013). New insights into the classification and nomenclature of cortical GABAergic interneurons. *Nature Reviews. Neuroscience*, *14*(3), 202–216. https://doi.org/10.1038/nrn3444

Donahue, C. J., Glasser, M. F., Preuss, T. M., Rilling, J. K., & Van Essen, D. C. (2018). Quantitative assessment of prefrontal cortex in humans relative to nonhuman primates. *Proceedings of the National Academy of Sciences of the United States of America*, *115*(22), E5183. https://doi.org/10.1073/pnas.1721653115

D'Souza, R. D., & Burkhalter, A. (2017). A Laminar Organization for Selective Cortico-Cortical Communication. *Frontiers in Neuroanatomy*, *11*, 71. https://doi.org/10.3389/fnana.2017.00071

Dzaja, D., Hladnik, A., Bičanić, I., Baković, M., & Petanjek, Z. (2014). Neocortical calretinin neurons in primates: Increase in proportion and microcircuitry structure. *Frontiers in Neuroanatomy*, *8*. https://doi.org/10.3389/fnana.2014.00103

Fuster, J. M. (2008a). Chapter 2—Anatomy of the Prefrontal Cortex. In J. M. Fuster (Ed.), *The Prefrontal Cortex (Fourth Edition)* (pp. 7–58). Academic Press. https://doi.org/10.1016/B978-0-12-373644-4.00002-5

Fuster, J. M. (2008b). Chapter 5—Human Neuropsychology. In J. M. Fuster (Ed.), *The Prefrontal Cortex (Fourth Edition)* (pp. 171–219). Academic Press. https://doi.org/10.1016/B978-0-12-373644-4.00005-0

Gabbott, P. L. A. (n.d.). *Local circuit neurons in the medial prefrontal cortex (areas 24a,b,c, 25 and 32) in the monkey: I. Cell morphology and morphometrics*. 42.

Gabbott, P. L. A. (2016). "Subpial Fan Cell"—A Class of Calretinin Neuron in Layer 1 of Adult Monkey Prefrontal Cortex. *Frontiers in Neuroanatomy*, *10*. https://doi.org/10.3389/fnana.2016.00028

Gabbott, P. L. A., Dickie, B. G. M., Vaid, R. R., Headlam, A. J. N., & Bacon, S. J. (n.d.). *Local-circuit neurones in the medial prefrontal cortex (areas 25, 32 and 24b) in the rat: Morphology and quantitative distribution*. 35.

Gabbott, P. L. A., Jays, P. R. L., & Bacon, S. J. (n.d.). *Calretinin Neurons in Human Medial Prefrontal Cortex (Areas 24a,b,c, 328, and 25)*. 22.

Gabbott, P. L., & Bacon, S. J. (1996). Local circuit neurons in the medial prefrontal cortex (areas 24a,b,c, 25 and 32) in the monkey: I. Cell morphology and morphometrics. *The Journal of Comparative Neurology*, *364*(4), 567–608. PubMed.

https://doi.org/10.1002/(SICI)1096-9861(19960122)364:4<567::AID-CNE1>3.0.CO;2-1

Gasnier, B. (2004). The SLC32 transporter, a key protein for the synaptic release of inhibitory amino acids. *Pflugers Archiv : European Journal of Physiology*, *447*(5), 756–759. PubMed. https://doi.org/10.1007/s00424-003-1091-2

Gilman, J. P., Medalla, M., & Luebke, J. I. (2016). Area-Specific Features of Pyramidal Neurons—A Comparative Study in Mouse and Rhesus Monkey. *Cerebral Cortex, 27*(3), 2078–2094. https://doi.org/10.1093/cercor/bhw062

Gonchar, Y., & Burkhalter, A. (2003). Distinct GABAergic Targets of Feedforward and Feedback Connections Between Lower and Higher Areas of Rat Visual Cortex. *The Journal of Neuroscience*, *23*(34), 10904–10912. https://doi.org/10.1523/JNEUROSCI.23-34-10904.2003

Gonzalez-Burgos, G., Cho, R. Y., & Lewis, D. A. (2015). Alterations in Cortical Network Oscillations and Parvalbumin Neurons in Schizophrenia. *Biological Psychiatry*, *77*(12), 1031–1040. https://doi.org/10.1016/j.biopsych.2015.03.010

Grant, P. (2015). Cerebral Cortex. In J. D. Wright (Ed.), *International Encyclopedia of the Social & Behavioral Sciences (Second Edition)* (pp. 332–343). Elsevier. https://doi.org/10.1016/B978-0-08-097086-8.55009-0

Hässler, R., & Stephen, Thieme. (1967). Comparative Anatomy of the Central Visual System in Day- and Night-Active Primates. *Evolution of the Forebrain*.

Hattori, R., Kuchibhotla, K. V., Froemke, R. C., & Komiyama, T. (2017). Functions and dysfunctions of neocortical inhibitory neuron subtypes. *Nature Neuroscience*, *20*(9), 1199–1208. https://doi.org/10.1038/nn.4619

Hladnik, A., Džaja, D., Darmopil, S., Jovanov-Milošević, N., & Petanjek, Z. (2014). Spatio-temporal extension in site of origin for cortical calretinin neurons in primates. *Frontiers in Neuroanatomy*, *8*, 50. https://doi.org/10.3389/fnana.2014.00050

Hsu, A., Luebke, J. I., & Medalla, M. (2017). Comparative ultrastructural features of excitatory synapses in the visual and frontal cortices of the adult mouse and monkey. *Journal of Comparative Neurology*, *525*(9), 2175–2191. https://doi.org/10.1002/cne.24196

Ingram, T. G. J., King, J. L., & Crowder, N. A. (2019). Divisive inhibition prevails during simultaneous optogenetic activation of all interneuron subtypes in mouse primary visual cortex. *Frontiers in Neural Circuits*, *13*, 40. https://doi.org/10.3389/fncir.2019.00040

Kawaguchi, Y., Otsuka, T., Morishima, M., Ushimaru, M., & Kubota, Y. (2019). Control of excitatory hierarchical circuits by parvalbumin-FS basket cells in layer 5 of the frontal cortex: Insights for cortical oscillations. *Journal of Neurophysiology*, *121*(6), 2222–2236. https://doi.org/10.1152/jn.00778.2018

Kirkcaldie, M. T. K. (2012). Chapter 4—Neocortex. In C. Watson, G. Paxinos, & L. Puelles (Eds.), *The Mouse Nervous System* (pp. 52–111). Academic Press. https://doi.org/10.1016/B978-0-12-369497-3.10004-4

Kisvárday, Z. F., Ferecskó, A. S., Kovács, K., Buzás, P., Budd, J. M. L., & Eysel, U. T. (2002). One axon-multiple functions: Specificity of lateral inhibitory connections by large basket cells. *Journal of Neurocytology*, *31*(3–5), 255–264. PubMed. https://doi.org/10.1023/a:1024122009448

Klausberger, T., Magill, P. J., Márton, L. F., Roberts, J. D. B., Cobden, P. M., Buzsáki, G., & Somogyi, P. (2003). Brain-state- and cell-type-specific firing of hippocampal interneurons in vivo. *Nature*, *421*(6925), 844–848. https://doi.org/10.1038/nature01374

Knowles, W. D., & Schwartzkroin, P. A. (1981). Local circuit synaptic interactions in hippocampal brain slices. *Journal of Neuroscience*, *1*(3), 318–322. https://doi.org/10.1523/JNEUROSCI.01-03-00318.1981

Kubota, Y., Kondo, S., Nomura, M., Hatada, S., Yamaguchi, N., Mohamed, A. A., Karube, F., Lübke, J., & Kawaguchi, Y. (2015). Functional effects of distinct innervation styles of pyramidal cells by fast spiking cortical interneurons. *ELife*, *4*, e07919. https://doi.org/10.7554/eLife.07919

Laramée, M.-E., & Boire, D. (2015). Visual cortical areas of the mouse: Comparison of parcellation and network structure with primates. *Frontiers in Neural Circuits*, *8*. https://doi.org/10.3389/fncir.2014.00149

Laubach, M., Amarante, L. M., Swanson, K., & White, S. R. (2018). What, if anything, is rodent prefrontal cortex? *Eneuro*, *5*(5), ENEURO.0315-18.2018. https://doi.org/10.1523/ENEURO.0315-18.2018

Luebke, J. I. (2017). Pyramidal neurons are not generalizable building blocks of cortical networks. *Frontiers in Neuroanatomy*, *11*. https://doi.org/10.3389/fnana.2017.00011

Luo, H., Hasegawa, K., Liu, M., & Song, W.-J. (2017). Comparison of the upper marginal neurons of cortical layer 2 with layer 2/3 pyramidal neurons in mouse temporal cortex. *Frontiers in Neuroanatomy*, *11*, 115–115. PubMed. https://doi.org/10.3389/fnana.2017.00115

Medalla, M., Gilman, J. P., Wang, J.-Y., & Luebke, J. I. (2017). Strength and diversity of inhibitory signaling differentiates primate anterior cingulate from lateral prefrontal cortex. *The Journal of Neuroscience*, *37*(18), 4717. https://doi.org/10.1523/JNEUROSCI.3757-16.2017

Melchitzky, D. S., Eggan, S. M., & Lewis, D. A. (2005). Synaptic targets of calretinin-containing axon terminals in macaque monkey prefrontal cortex. *Neuroscience*, *130*(1), 185–195. https://doi.org/10.1016/j.neuroscience.2004.08.046

Meskenaite, V. (1997). Calretinin-immunoreactive local circuit neurons in area 17 of the cynomolgus monkey, Macaca fascicularis. *Journal of Comparative Neurology*, *379*(1), 113–132. https://doi.org/10.1002/(SICI)1096-9861(19970303)379:1<113::AID-CNE8>3.0.CO;2-7

Petrides, M. (2014). Cytoarchitecture. In *Neuroanatomy of Language Regions of the Human Brain* (pp. 89–138). Academic Press. https://doi.org/10.1016/B978-0-12-405514-8.50005-0

Pierri, J. N., Chaudry, A. S., Woo, T.-U. W., & Lewis, D. A. (1999). Alterations in chandelier neuron axon terminals in the prefrontal cortex of schizophrenic subjects. *American Journal of Psychiatry*, *156*(11), 1709–1719. https://doi.org/10.1176/ajp.156.11.1709

Povysheva, N. V., Zaitsev, A. V., Rotaru, D. C., Gonzalez-Burgos, G., Lewis, D. A., & Krimer, L. S. (2008). Parvalbumin-positive basket interneurons in monkey and rat prefrontal cortex. *Journal of Neurophysiology*, *100*(4), 2348–2360. https://doi.org/10.1152/jn.90396.2008

Rose, J. E., & Woolsey, C. N. (1948). Structure and relations of limbic cortex and anterior thalamic nuclei in rabbit and cat. *The Journal of Comparative Neurology*, *89*(3), 279–347. PubMed. https://doi.org/10.1002/cne.900890307

Rudy, B., Fishell, G., Lee, S., & Hjerling-Leffler, J. (2011). Three groups of interneurons account for nearly 100% of neocortical GABAergic neurons. *Developmental Neurobiology*, *71*(1), 45–61. https://doi.org/10.1002/dneu.20853

Runyan, C. A., Schummers, J., Van Wart, A., Kuhlman, S. J., Wilson, N. R., Huang, Z. J., & Sur, M. (2010). Response features of parvalbumin-expressing interneurons suggest precise roles for subtypes of inhibition in visual cortex. *Neuron*, *67*(5), 847–857. https://doi.org/10.1016/j.neuron.2010.08.006

Saffari, R., Grotefeld, K., Kravchenko, M., Zhang, M., & Zhang, W. (2019). Calretinin+-neurons-mediated GABAergic inhibition in mouse prefrontal cortex. *Progress in Neuro-Psychopharmacology and Biological Psychiatry*, *94*, 109658. https://doi.org/10.1016/j.pnpbp.2019.109658

Schneider, C. A., Rasband, W. S., & Eliceiri, K. W. (2012). NIH Image to ImageJ: 25 years of image analysis. *Nature Methods*, *9*(7), 671–675. https://doi.org/10.1038/nmeth.2089

Senzai, Y., Fernandez-Ruiz, A., & Buzsáki, G. (2019). Layer-specific physiological features and interlaminar interactions in the primary visual cortex of the mouse. *Neuron*, *101*(3), 500–513.e5. https://doi.org/10.1016/j.neuron.2018.12.009

Somogyi, P., & Klausberger, T. (2005). Defined types of cortical interneurone structure space and spike timing in the hippocampus. *The Journal of Physiology*, *562*(1), 9–26. https://doi.org/10.1113/jphysiol.2004.078915

Tamamaki, N., Yanagawa, Y., Tomioka, R., Miyazaki, J.-I., Obata, K., & Kaneko, T. (2003). Green fluorescent protein expression and colocalization with calretinin, parvalbumin, and somatostatin in the GAD67-GFP knock-in mouse. *The Journal of Comparative Neurology*, *467*(1), 60–79. https://doi.org/10.1002/cne.10905

Tomioka, R., & Rockland, K. S. (2007). Long-distance corticocortical GABAergic neurons in the adult monkey white and gray matter. *The Journal of Comparative Neurology*, *505*(5), 526–538. PubMed. https://doi.org/10.1002/cne.21504

Xu, X., Olivas, N. D., Ikrar, T., Peng, T., Holmes, T. C., Nie, Q., & Shi, Y. (2016). Primary visual cortex shows laminar-specific and balanced circuit organization of excitatory and inhibitory synaptic connectivity. *The Journal of Physiology*, *594*(7), 1891–1910. https://doi.org/10.1113/JP271891

Zaitsev, A. V., Gonzalez-Burgos, G., Povysheva, N. V., Kröner, S., Lewis, D. A., & Krimer, L. S. (2005). Localization of calcium-binding proteins in physiologically

and morphologically characterized interneurons of monkey dorsolateral prefrontal cortex. *Cerebral Cortex*, *15*(8), 1178–1186. https://doi.org/10.1093/cercor/bhh218

Zhang, Z.-W., & Deschênes, M. (1997). Intracortical axonal projections of lamina VI cells of the primary somatosensory cortex in the rat: A single-cell labeling study. *The Journal of Neuroscience*, *17*(16), 6365. https://doi.org/10.1523/JNEUROSCI.17-16-06365.1997

CURRICULUM VITAE